JACS
JOURNAL OF THE AMERICAN CHEMICAL SOCIETY

ARTICLE

pubs.acs.org/JACS

Toward Functional Carboxylate-Bridged Diiron Protein Mimics: Achieving Structural Stability and Conformational Flexibility Using a Macrocylic Ligand Framework

Loi H. Do and Stephen J. Lippard*

Department of Chemistry, Massachusetts Institute of Technology, Cambridge, Massachusetts 02139, United States

Supporting Information

ABSTRACT: A dinucleating macrocycle, H_2PIM, containing phenoxylimine metal-binding units has been prepared. Reaction of H_2PIM with $[Fe_2(Mes)_4]$ (Mes = 2,4,6-trimethylphenyl) and sterically hindered carboxylic acids, Ph_3CCO_2H or $Ar^{Tol}CO_2H$ (2,6-bis(*p*-tolyl)benzoic acid), afforded complexes $[Fe_2(PIM)(Ph_3CCO_2)_2]$ (**1**) and $[Fe_2(PIM)(Ar^{Tol}CO_2)_2]$ (**2**), respectively. X-ray diffraction studies revealed that these diiron(II) complexes closely mimic the active site structures of the hydroxylase components of bacterial multicomponent monooxygenases (BMMs), particularly the syn disposition of the nitrogen donor atoms and the bridging μ-$\eta^1\eta^2$ and μ-$\eta^1\eta^1$ modes of the carboxylate ligands at the diiron(II) centers. Cyclic voltammograms of **1** and **2** displayed quasi-reversible redox couples at +16 and +108 mV vs ferrocene/ferrocenium, respectively. Treatment of **2** with silver perchlorate afforded a silver(I)/iron(III) heterodimetallic complex, $[Fe_2(\mu\text{-}OH)_2(ClO_4)_2(PIM)(Ar^{Tol}CO_2)Ag]$ (**3**), which was structurally and spectroscopically characterized. Complexes **1** and **2** both react rapidly with dioxygen. Oxygenation of **1** afforded a (μ-hydroxo)diiron(III) complex $[Fe_2(\mu\text{-}OH)(PIM)(Ph_3CCO_2)_3]$ (**4**), a hexa(μ-hydroxo)-tetrairon(III) complex $[Fe_4(\mu\text{-}OH)_6(PIM)_2(Ph_3CCO_2)_2]$ (**5**), and an unidentified iron(III) species. Oxygenation of **2** exclusively formed di(carboxylato)diiron(III) compounds, a testimony to the role of the macrocylic ligand in preserving the dinuclear iron center under oxidizing conditions. X-ray crystallographic and ^{57}Fe Mössbauer spectroscopic investigations indicated that **2** reacts with dioxygen to give a mixture of (μ-oxo)diiron(III) $[Fe_2(\mu\text{-}O)(PIM)(Ar^{Tol}CO_2)_2]$ (**6**) and di(μ-hydroxo)diiron(III) $[Fe_2(\mu\text{-}OH)_2(PIM)(Ar^{Tol}CO_2)_2]$ (**7**) units in the same crystal lattice. Compounds **6** and **7** spontaneously convert to a tetrairon(III) complex, $[Fe_4(\mu\text{-}OH)_6(PIM)_2(Ar^{Tol}CO_2)_2]$ (**8**), when treated with excess H_2O.

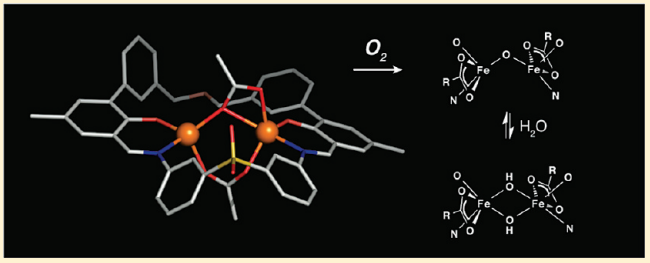

INTRODUCTION

Bacterial multicomponent monooxygenases (BMMs) are a remarkable family of enzymes that catalyze the oxidation of aliphatic and aromatic hydrocarbons using the naturally abundant molecule O_2.[1,2] They include soluble methane monooxygenase (sMMO),[3] toluene/*o*-xylene monooxygenase (ToMO),[4−6] phenol hydroxylase (PH),[7] and alkene monooxygenase (AMO),[8] among others.[9,10] Extensive structural studies revealed that the active sites of these enzymes contain a non-heme diiron center located within a hydrophobic four-helix bundle. The reduced form of sMMO hydroxylase ($sMMOH_{red}$) has a diiron(II) core coordinated by four carboxylate amino acid side chains, two bridging and two terminal, and two imidazole groups syn with respect to the Fe−Fe vector (Scheme 1).[11−13] This carboxylate-bridged diiron motif is ubiquitous in biology and is believed to be an essential component in several mammalian proteins.[14−16] Understanding the chemistry that occurs at these bioinorganic cofactors has far-reaching implications for human health as well as for environmental remediation[17−19] and chemical synthesis.[20−23]

Developing a functional model of the BMM active site is a formidable challenge.[24−28] In addition to matching the identity and geometric arrangement of ligands at the diiron(II) center, the model complex must be structurally stable yet conformationally flexible upon reaction with O_2 and other substrates. In the enzyme, this balance is achieved by a rigid active site structure that enforces the dinuclearity of the metal centers but allows shifting of the carboxylate ligations to accommodate entry of guest molecules.[11,29] The most common strategy for assembling discrete diiron compounds is to react Fe(II) or Fe(III) salts with simple polydentate ligands.[25,30] Although some of these complexes are excellent structural and spectroscopic models for the biological cofactor,[31−34] they either exhibit poor dioxygen reactivity or do not give rise to reactive oxygenated species.[35,36] Given the extent of today's synthetic toolbox, it should be possible to prepare more sophisticated synthetic compounds that can mimic various functional aspects of the biological diiron unit.[26]

In a significant step toward achieving this objective, we employed a de novo approach to construct a diiron model complex that mimics features of the BMM active sites. The "primary" ligand must support a diiron core in multiple oxidation

Received: March 8, 2011
Published: June 17, 2011

dx.doi.org/10.1021/ja2021312 | *J. Am. Chem. Soc.* 2011, 133, 10568–10581

Scheme 1. Reaction of the Diiron(II) Complex of Soluble Methane Monooxygenase Hydroxylase ($sMMOH_{red}$) with Dioxygen and Saturated Hydrocarbons (RH) To Give Alcohols (ROH) and the Resting Diiron(III) State of the Protein ($sMMOH_{ox}$)[a]

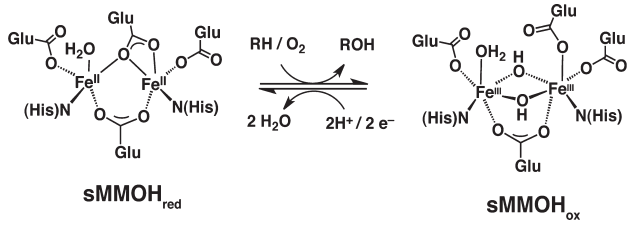

$sMMOH_{red}$ $sMMOH_{ox}$

[a] $sMMOH_{ox}$ can be reduced back to $sMMOH_{red}$ by acquiring two electrons from a reductase protein (sMMOR). The active site structures of $sMMOH_{red}$ and $sMMOH_{ox}$ are depicted.

Chart 1. Syn *N*-Donor Ligands Containing Mixed *N,O* Metal Binding Units[a]

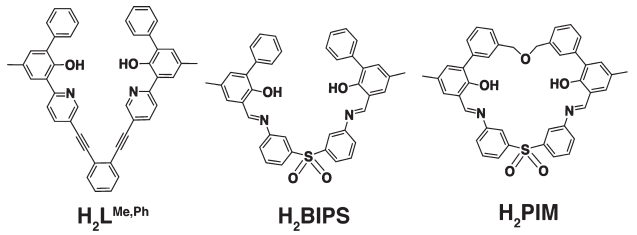

$H_2L^{Me,Ph}$ H_2BIPS H_2PIM

[a] Compounds $H_2L^{Me,Ph}$ and H_2BIPS spontaneously assemble into bis(ligand) diiron complexes in the presence of base and iron(II) salts. The macrocyclic variant H_2PIM was designed to have a flexible ether linkage to prevent ligand interdigitation upon metal complexation.

states, enforce syn *N*-stereochemistry of nitrogen donors, have two anionic oxygen atom donors, allow binding of two external carboxylates to the iron centers, have an internal cavity to form a quadrilateral $Fe_2(\mu\text{-}O)_2$ core, and be readily synthesized in gram quantities. Our initial studies using covalently linked *N*-donor ligands were promising,[37,38] but the diiron(II) complexes prepared either were too kinetically labile or contained two interdigitated syn *N*-donor units rather than one.[39,40] We overcame the previously encountered difficulties by designing a new macrocylic ligand, H_2PIM, containing phenoxylimine metal binding groups (Chart 1). We used H_2PIM and sterically hindered carboxylates to synthesize structural models of the carboxylate-bridged diiron active sites of the BMMs and related enzymes. We show that PIM^{2-}, the doubly deprotonated form of H_2PIM, has all the characteristics that were engineered into the ligand design and imparts stability to the diiron unit, even following reactions with O_2. Although a functional protein mimic has not yet been achieved, this work demonstrates that more advanced diiron model complexes can be prepared using tailor-made macrocyclic ligand platforms, thus providing a new conceptual framework with which to guide future biomimetic studies.

EXPERIMENTAL SECTION

Materials and Methods. Reagents obtained from Strem, Aldrich Chemical Co., and Alfa Aesar were used as received. Synthetic procedures for compounds **A**−**D** are provided in the SI. The compounds 2,6-bis(*p*-tolyl)benzoic acid[41] ($Ar^{Tol}CO_2H$, also referred to as terphenylcarboxylic acid for simplicity) and $[Fe_2(Mes)_4]$[42] (Mes = 2,4,6-trimethylphenyl) were prepared as reported. All ^{57}Fe-enriched compounds were prepared exactly as described for the unenriched analogues, except that $[^{57}Fe_2(Mes)_4]$ was used as the starting material. All air-sensitive manipulations were performed using standard Schlenk techniques or under a nitrogen atmosphere inside an MBraun drybox. Solvents were saturated with argon and purified by passage through two columns of activated alumina. Dioxygen gas used in these experiments was obtained from a high-purity gas cylinder (Airgas) and passed through a 10-in. column of activated alumina before use.

General Physical Methods. NMR spectra were recorded on 500 MHz Varian Mercury spectrometers, and chemical shifts for ^{1}H and ^{13}C (proton-decoupled) NMR spectra were referenced to residual solvent. ^{1}H NMR spectral data of paramagnetic compounds were obtained by widening the sweep window (+100 to −30 ppm) and collecting for longer acquisition times (~1024 scans). IR spectra were recorded on a ThermoNicolet Avatar 360 spectrophotometer with the OMNIC software. Absorption spectra were recorded on a Cary 50 spectrophotometer using 6Q Spectrosil quartz cuvettes (Starna) with 1 cm path lengths. X-band EPR spectra were recorded at 5 K on a Bruker EMX spectrometer. Electrochemical measurements were performed with a VersaSTAT3 Princeton Applied Research potentiostat running the V3-Studio electrochemical analysis software. A three-electrode setup was employed comprising a platinum working electrode, a platinum wire auxiliary electrode, and a 0.1 M $Ag/AgNO_3$ solution in acetonitrile as the reference electrode. Tetra-*n*-butylammonium hexafluorophosphate (0.1 M) was used as the supporting electrolyte. Electrochemical potentials are referenced externally to the ferrocene/ferrocenium couple at 0.00 V.

X-ray Data Collection and Refinement. Single crystals were mounted in Paratone oil using 30 μm aperture MiTeGen MicroMounts (Ithaca, NY) and frozen under a 100 K KRYO-FLEX nitrogen cold stream. Data were collected on a Bruker SMART APEX CCD X-ray diffractometer with Mo Kα radiation (λ = 0.71073 Å) controlled by the APEX 2 (v. 2010.1-2) software package. Data reduction was performed using SAINT and empirical absorption corrections were applied using SADABS.[43] The structures were solved by Patterson methods with refinement by full-matrix least squares based on F^2 using the SHELXTL-97 software package[44] and checked for higher symmetry by the PLATON software.[45] All non-hydrogen atoms were located and refined anisotropically. Hydrogen atoms were fixed to idealized positions unless otherwise noted and given thermal parameters equal to either 1.5 (methyl hydrogen atoms) or 1.2 (non-methyl hydrogen atoms) times the thermal parameters of the atoms to which they are attached. Additional X-ray crystallographic details are provided in the Supporting Information (SI).

^{57}Fe Mössbauer Spectroscopy. Mössbauer spectra were recorded on an MSI spectrometer (WEB Research Co.) with a ^{57}Co source in a Rh matrix maintained at room temperature. Solid samples were prepared by suspension of the complex (~5−40 mg, depending on whether the complex is enriched in ^{57}Fe) in Apiezon M grease and placed in a nylon sample holder. Solution samples were prepared by freezing 400 μL of the complex (~20 mM) in a nylon sample cup and sealing with a screw cap. Samples containing natural abundance iron were measured over the course of ~5 d, whereas samples that are enriched in ^{57}Fe were collected over ~12 h. Data were acquired at 80 K, and isomer shift (δ) values are reported with respect to metallic iron that was used for velocity calibration at room temperature. Spectra were fit to Lorentzian lines using the WMOSS plot-and-fit program.

Syntheses. *H_2PIM.* Compound **D** (1.70 g, 3.65 mmol) was dissolved in 10 mL of dichloromethane and combined with 3,3′-diaminodiphenylsulfone (0.900 g, 3.65 mmol) in 700 mL of dry acetonitrile. About 1 mL of trifluoroacetic acid was added, and the mixture was refluxed for

6 h. Over the course of ~1 h, a large amount of bright yellow-orange material formed. The solid was isolated by filtration and washed with diethyl ether to afford analytically pure product (1.80 g, 72%). ^{1}H NMR ($CDCl_3$, 500 MHz): δ 13.16 (s, 2H), 8.63 (s, 2H), 7.89 (d, J = 9.5 Hz, 2H), 7.80 (m, 2H), 7.73 (s, 2H), 7.67 (t, J = 8.0 Hz, 2H), 7.44 (m, 4H), 7.39 (m, 4H), 7.28 (m, 2H), 7.21 (s, 2H), 4.69 (s, 4H), 2.36 (s, 6H) ppm. ^{13}C NMR ($CDCl_3$, 125 MHz): δ 164.78, 156.69, 149.82, 143.08, 138.09, 137.72, 136.08, 132.20, 130.72, 130.32, 129.57, 128.69, 128.51, 128.30, 127.06, 125.30, 123.73, 123.59, 118.85, 73.03, 20.61 ppm. IR (KBr): ν 2852, 1620, 1579, 1472, 1454, 1427, 1326, 1302, 1211, 1148, 1092, 886, 783, 700, 689, 620, 524 cm^{-1}. DART-MS(−) = 677.2121 (calcd = 677.2116 [M−H]$^-$). Mp = 313−315 °C.

*[Fe$_2$(PIM)(Ph$_3$CCO$_2$)$_2$] (**1**).* In an anaerobic drybox, solid H_2PIM (100 mg, 147 μmol) and triphenylacetic acid (85.0 mg, 295 μmol) were dissolved in 2.0 mL of tetrahydrofuran. A 1.0 mL solution of tetrahydrofuran containing [Fe$_2$(Mes)$_4$] (86.0 mg, 147 μmol) was added to the reaction vessel, and the mixture was stirred for 1 h. The dark red solution was evaporated to dryness, and the residue was redissolved in benzene. The solution was filtered through a glass wool plug and layered with pentane. After ~12 h, a large amount of red crystals had formed that were suitable for X-ray diffraction analysis. The solid material was isolated by filtration and washed with pentane to give the desired diiron complex (171 mg, 86%). ^{1}H NMR (C_6D_6, 500 MHz): δ 78.37, 74.97, 48.27, 22.78, 8.20−1.19, −5.32, −6.20, −10.37, −13.49, −21.13 ppm. IR (KBr): ν 3056, 3031, 2918, 2850, 1578, 1545, 1490, 1444, 1418, 1378, 1322, 1304, 1284, 1200, 1175, 1152, 1097, 1085, 1036, 985, 790, 745, 699, 673, 547 cm^{-1}. UV−vis (CH_2Cl_2): λ_{max} = 290 (36 300 M^{-1} cm^{-1}), 410 (16 000 M^{-1} cm^{-1}) nm. Anal. Calcd for $Fe_2C_{82}H_{62}N_2O_9S\cdot(C_4H_8O)$ (**1**·THF): C, 71.97; H, 4.92; N, 1.95. Found: C, 71.80; H, 4.94; N, 2.22. Mp (decomp) = 302 °C. Mössbauer (polycrystalline, apiezon M grease): δ_1 = 1.18(2) mm/s, ΔE_{Q1} = 2.33(2) mm/s, $\Gamma_{L/R(1)}$ = 0.38(2) mm/s, Site 1 Area = 53%; δ_2 = 0.97(2) mm/s, ΔE_{Q2} = 2.25(2) mm/s, $\Gamma_{L/R(2)}$ = 0.35(2) mm/s, Site 2 Area = 47%.

*[Fe$_2$(PIM)(Ar^{Tol}CO$_2$)$_2$] (**2**).* The synthesis of [Fe$_2$(PIM)(Ar^{Tol}CO$_2$)$_2$] was performed as described for [Fe$_2$(PIM)(Ph$_3$CCO$_2$)$_2$] (**1**), except that Ar^{Tol}CO$_2$H was used instead of Ph$_3$CCO$_2$H. The product crystallized upon slow diffusion of pentane into a solution of the complex in dichloromethane and was isolated as a red powder when dried (152 mg, 74%). X-ray diffraction quality crystals were readily obtained by slow diffusion of pentane into a dichloromethane solution of the complex. ^{1}H NMR (CD_2Cl_2, 500 MHz): δ 76.92, 73.82, 49.00, 24.68, 7.86, 7.31, 6.22, 2.41, 1.37, 0.96, −0.41, −1.81, −5.72, −9.04, −19.60 ppm. IR (KBr): ν 3052, 3024, 2912, 2851, 1614, 1577, 1533, 1445, 1413, 1381, 1302, 1286, 1202, 1149, 1073, 819, 791, 712, 695, 542 cm^{-1}. UV−vis (CH_2Cl_2): λ_{max} = 290 (36 700 M^{-1} cm^{-1}), 418 (14 000 M^{-1} cm^{-1}) nm. Anal. Calcd for $Fe_2C_{84}H_{66}N_2O_9S\cdot(C_4H_8O)$ (**2**·THF): C, 72.23; H, 5.10; N, 1.91. Found: C, 71.72; H, 4.92; N, 2.17. Mp (decomp) = 240 °C. Mössbauer (polycrystalline, apiezon M grease): δ_1 = 1.10(2) mm/s, ΔE_{Q1} = 2.04(2) mm/s, $\Gamma_{L/R(1)}$ = 0.38(2) mm/s, Site 1 Area = 63%; δ_2 = 0.95(2) mm/s, ΔE_{Q2} = 2.02(2) mm/s, $\Gamma_{L/R(2)}$ = 0.32(2) mm/s, Site 2 Area = 37%.

*[Fe$_2$(μ-OH)$_2$(ClO$_4$)$_2$(PIM)(Ar^{Tol}CO$_2$)Ag] (**3**).* In an anaerobic drybox, [Fe$_2$(PIM)(Ar^{Tol}CO$_2$)$_2$] (**2**) (19 mg, 14 μmol) and silver perchlorate (10 mg, 48 μmol) were combined in 2 mL of dichloromethane and stirred for 1 h. The reaction mixture was filtered through a glass wool plug to remove a black precipitate. The solution was concentrated to half its volume and layered with 0.5 mL of pentane. After ~14 h, a dark solid formed on the bottom of the reaction vial. This product was isolated by filtration, yielding a dark crystalline solid (15 mg, 76%). Crystals suitable for X-ray diffraction studies were obtained by slow diffusion of pentane into a solution of the complex in dichloromethane. IR (KBr): ν 3432, 2919, 2851, 1579, 1546, 1521, 1472, 1446, 1382, 1337, 1306, 1285, 1200, 1181, 1152, 1122, 1020, 796, 603, 548, 530 cm^{-1}. UV−vis (CH_2Cl_2): λ_{max} = 290 (32 300 M^{-1} cm^{-1}), 375 (11 100 M^{-1} cm^{-1}), 479 (sh, 3300 M^{-1} cm^{-1}), 600 (2300 M^{-1} cm^{-1}). Anal. Calcd for $Fe_2C_{63}H_{51}AgCl_2N_2O_{17}S\cdot(CH_2Cl_2)$ (**3**·CH_2Cl_2): C, 50.72; H, 3.52; N, 1.85; Cl, 9.36. Found: C, 51.04; H, 3.64; N, 1.77; Cl, 9.23. Mp (decomp) ≈ 270 °C. Mössbauer (THF): δ = 0.49(2) mm/s, ΔE_Q = 1.38(2) mm/s, $\Gamma_{L/R}$ = 0.56(2) mm/s.

*[Fe$_2$(μ-OH)(PIM)(Ph$_3$CCO$_2$)$_3$] (**4**).* In an anaerobic drybox, solid [Fe$_2$(PIM)(Ph$_3$CCO$_2$)$_2$] (**1**) (30 mg, 22 μmol), triphenylacetic acid (13 mg, 44 μmol), and triethylamine (6.0 μL) were combined in 2.0 mL of benzene. The reaction vial was sealed with a septum, brought outside of the glovebox, and bubbled with dioxygen for 5 min. When exposed to O_2, the clear red solution quickly turned dark brown. Upon vapor diffusion of pentane into the benzene solution, several large X-ray diffraction quality crystals were obtained. The product was isolated by filtration (8 mg, 22%). ^{1}H NMR ($CDCl_3$, 500 MHz): δ 51.28, 44.24, 33.02, 29.70, 23.90, 6.60, −4.52, −7.85 ppm. IR (KBr): ν 3438, 3056, 3032, 2919, 1582, 1544, 1491, 1477, 1446, 1405, 1373, 1331, 1205, 1150, 1035, 827, 789, 744, 699, 677, 642, 604, 547, 523 cm^{-1}. UV−vis (CH_2Cl_2): λ_{max} = 284 (108 000 M^{-1} cm^{-1}), 372 (38 000 M^{-1} cm^{-1}), and 570 (10 300 M^{-1} cm^{-1}) nm. Anal. Calcd for $Fe_2C_{102}H_{78}N_2O_{12}S\cdot(C_6H_6)\cdot(NC_6H_{15})_2$ (**4**·C_6H_6·$(NEt_3)_2$): C, 73.99; H, 5.90; N, 2.88. Found: C, 74.40; H, 5.66; N, 3.22. Mp = 214−217 °C. Mössbauer (polycrystalline, apiezon M grease): δ = 0.52(2) mm/s, ΔE_Q = 0.95(2) mm/s, $\Gamma_{L/R}$ = 0.38(2) mm/s.

*[Fe$_4$(μ-OH)$_6$(PIM)$_2$(Ph$_3$CCO$_2$)$_2$] (**5**).* In an anaerobic drybox, solid [Fe$_2$(PIM)(Ph$_3$CCO$_2$)$_2$] (**1**) (40 mg, 29 μmol) was combined with 2.0 mL of benzene in a septum-sealed reaction vessel. Dioxygen was bubbled through the mixture for 5 min. The solution was concentrated to approximately half its volume and then left alone to crystallize over ~1 d by slow evaporation. This method resulted in selective crystallization of the desired tetranuclear [Fe$_4$(μ-OH)$_6$(PIM)$_2$(Ph$_3$CCO$_2$)$_2$] (**5**) (hexagonal prisms) instead of the dinuclear [Fe$_2$(μ-OH)(PIM)(Ph$_3$CCO$_2$)$_3$] (**4**) (rectangular blocks). Crystals obtained from this method were suitable for X-ray diffraction studies. The desired product was isolated by filtration (10 mg, 32%). ^{1}H NMR ($CDCl_3$, 500 MHz): δ 49.97, 43.69, 31.24, 15.60, 8.71, 5.94, 5.31, 4.14, −7.12 ppm. IR (NaCl): ν 3554, 3445, 3064, 2961, 2921, 2850, 1580, 1542, 1381, 1340, 1324, 1260, 1238, 1204, 1151, 1101, 1080, 1017, 984, 800, 789, 747, 738, 705, 692, 671, 633, 528, 416 cm^{-1}. UV−vis (CH_2Cl_2): λ_{max} = 280 (84 200 M^{-1} cm^{-1}), 370 (25 000 M^{-1} cm^{-1}), and 540 (8060 M^{-1} cm^{-1}) nm. Anal. Calcd for $Fe_4C_{124}H_{100}N_4O_{20}S_2$ (**5**): C, 66.09; H, 4.47; N, 2.49. Found: C, 66.09; H, 4.50; N, 2.14. Mp (decomp) > 300 °C. Mössbauer (polycrystalline, apiezon M grease): δ = 0.51(2) mm/s, ΔE_Q = 1.06(2) mm/s, $\Gamma_{L/R}$ = 0.40(2) mm/s.

*[Fe$_2$(μ-O)(PIM)(Ar^{Tol}CO$_2$)$_2$] (**6**)/[Fe$_2$(μ-OH)$_2$(PIM)(Ar^{Tol}CO$_2$)$_2$] (**7**).* In an anaerobic drybox, [Fe$_2$(PIM)(Ar^{Tol}CO$_2$)$_2$] (**2**) (200 mg, 144 μmol) was dissolved in 2 mL of tetrahydrofuran in a 20 mL vial. The vial was sealed with a rubber septum and brought outside of the drybox. Dioxygen was bubbled through the reaction vial for 5 min, at which time the red solution became a dark brown. The tetrahydrofuran solvent was removed in vacuo, and the resulting brown solid (117 mg, 58%) was isolated and stored inside the drybox to prevent further reaction with ambient moisture. Single crystals suitable for X-ray diffraction analysis were obtained by slow diffusion of diethyl ether into a solution of the complex in acetonitrile. ^{1}H NMR ($CDCl_3$, 500 MHz): δ 26.30, 24.44, 21.84, 13.52, 15.92, 14.77, 11.56, 10.08, 9.58, 8.22, 5.44, 4.86, 4.26, 2.16, 1.80, 1.25, 0.88, −7.11 ppm. IR (KBr): ν 3448, 3021, 2918, 2856, 1613, 1582, 1545, 1515, 1473, 1448, 1383, 1336, 1304, 1286, 1205, 1152, 818, 791, 766, 700, 546, 531 cm^{-1}. UV−vis (CH_2Cl_2): λ_{max} = 380 (sh), 473, 600 nm. Anal. Calcd for $Fe_2C_{84}H_{68}N_2O_{11}S\cdot(CH_3CN)$ (**6**·CH_3CN): C, 70.45; H, 4.88; N, 2.87. Anal. Calcd for $Fe_2C_{84}H_{66}N_2O_{10}S\cdot(CH_3CN)$ (**7**·CH_3CN): C, 71.32; H, 4.80; N, 2.90. Found: C, 69.89; H, 4.76; N, 2.59. *As discussed in the text, compounds **6** and **7** exist as a mixture in the solid-state.* Mp (decomp) > 300 °C. Mössbauer (polycrystalline, apiezon M grease): δ_1 = 0.47(2) mm/s,

ΔE_{Q1} = 1.52(2) mm/s, $\Gamma_{L/R(1)}$ = 0.36(2) mm/s, Site 1 Area = 21%; δ_2 = 0.50(2) mm/s, ΔE_{Q2} = 0.97(2) mm/s, $\Gamma_{L/R(2)}$ = 0.48(2) mm/s, Site 2 Area = 79%.

*[$Fe_4(\mu$-OH)$_6$(PIM)$_2$($Ar^{Tol}CO_2$)$_2$] (**8**).* Solid [Fe_2(PIM)($Ar^{Tol}CO_2$)$_2$] (**2**) (200 mg, 144 μmol) was dissolved in 2.0 mL of benzene and stirred under dioxygen for 5 min, giving a dark brown solution. About 10 μL of water was then added to the reaction mixture, and the solution was stirred for an additional 10 min and then filtered through a glass wool plug before the filtrate was evaporated to dryness. The remaining solid was isolated as a pale brown material (~120 mg, 73%). ^{1}H NMR (DMF-d_7, 500 MHz): δ 72.80, 45.00, 26.24, 14.48, 13.26, 10.40, 7.30−0.12, −3.16, −4.65, −11.36 ppm. IR (KBr): ν 3432, 3019, 2919, 2857, 1614, 1584, 1543, 1516, 1473, 1450, 1385, 1324, 1304, 1286, 1206, 1151, 791, 703, 586, 528 cm^{-1}. UV−vis (CH_2Cl_2): λ_{max} = 360 (81 700 M^{-1} cm^{-1}), 550 (17 100 M^{-1} cm^{-1}) nm. Anal. Calcd for $Fe_4C_{126}H_{104}N_4O_{20}S_2\cdot(C_6H_6)_2$ (**8**·(C_6H_6)$_2$): C, 67.99; H, 4.80; N, 2.30. Found: C, 67.92; H, 4.80; N, 2.43. Mp (decomp) > 300 °C. Mössbauer (THF): δ = 0.49(2) mm/s, ΔE_Q = 0.97(2) mm/s, $\Gamma_{L/R}$ = 0.44(2) mm/s.

RESULTS AND DISCUSSION

Ligand Design and Synthesis. Our early attempts to prepare more accurate structural mimics of carboxylate-bridged diiron protein active sites led to the design of dinucleating ligands that enforce the syn stereochemistry of nitrogen donor atoms.[37,38] Studies using 1,2-bis(3-ethynyl-8-carboxylatequinoline)-4,5-diethylbenzene ethyl ester (Et_2BCQEB^{Et}) afforded a tri(μ-carboxylato)(syn *N*-donor)diiron(II) complex, which produced only an intractable mixture upon exposure to dioxygen. Other syn *N*-donor variants, such as $H_2L^{Me,Ph}$ and H_2BIPS (Chart 1), primarily afforded bis(ligand)diiron complexes formed through interdigitation of two dinucleating ligands when complexed with iron(II).[39,40]

To improve upon previous ligand designs, the macrocyclic compound H_2PIM was conceived (Chart 1). By linking the phenyl groups of H_2BIPS with a three-atom chain, H_2PIM still enforces syn arrangement of the nitrogen donors but has a more preorganized structure. We used phenolate and imine moieties instead of carboxylate and imidazole groups, respectively, because they confer both synthetic and functional advantages. Phenol is a versatile building block for constructing complex molecular architectures because its aromatic ring can be readily attached to other substituents.[46] Although the phenolate anion (pK_a of phenol ≈ 12−19 in DMSO) is more basic than a carboxylate (pK_a of carboxylic acid ≈ 9−13 in DMSO),[47,48] more electron-rich oxygen donors may stabilize iron in higher oxidation states, such as occurs in the diiron(IV) unit of intermediate Q.[49] Alternatively, the basicity of the phenolate groups can be lowered to better match the donor strength of Glu/Asp side chains by introducing electron-withdrawing substituents on PIM^{2-}. Tuning the pK_a value of the phenolate may also eliminate the possibility of forming ligand-centered radicals,[50] a potential barrier to accessing high-valent diiron species. An additional advantage of the phenolate ligand is that its iron complexes display visible absorption bands that provide a spectroscopic handle for studying otherwise optically silent species. Finally, imine groups are valuable in the H_2PIM framework because they form through Schiff base condensation reactions that are efficient in producing large macrocyclic structures with syn nitrogen donor atoms.[51,52]

The H_2PIM ligand was prepared as indicated in Scheme 2. The dibenzyl ether linker **A** was obtained by reaction of 3-bromobenzyl alcohol with sodium hydride, followed by refluxing with 3-bromobenzyl bromide. To prepare compound **B**, a palladium-catalyzed Negishi cross-coupling procedure was employed. After silica gel column chromatography, **B** was isolated as a colorless oil. Next, the tetrahydropyran protecting group of **B** was removed by treatment with oxalic acid in tetrahydrofuran/methanol to afford **C** as a white solid. Ortho formylation of **C** was achieved by treatment with anhydrous magnesium chloride, paraformaldehyde, and triethylamine to give **D** as a yellow oil. To obtain H_2PIM, **D** was condensed with 3,3′-diaminodiphenylsulfone, generating the desired product as a bright yellow-orange solid in good yield. The synthetic route for H_2PIM is amenable to scale-up, and the final ligand has been obtained in multigram quantities.

Scheme 2[a]

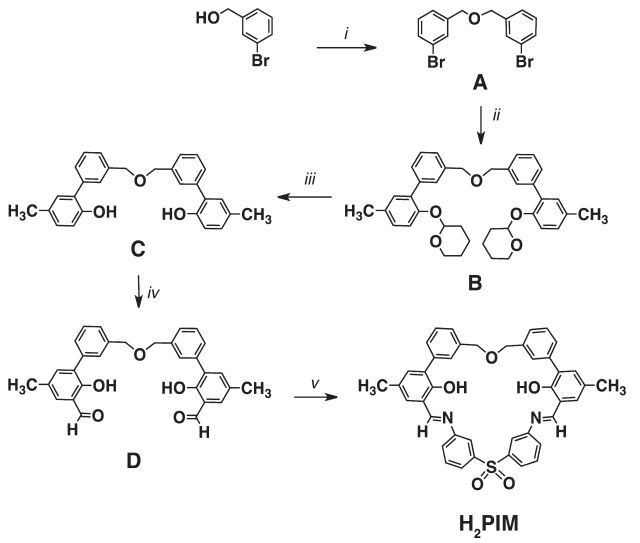

[a] Reagents and conditions: *i.* a) NaH, dry THF, b) 3-bromobenzylbromide. *ii.* a) Aryl zinc reagent: 2-(2-bromo-4-methylphenoxy)-tetrahydro-2*H*-pyran, *n*-butyllithium, $ZnCl_2$, THF, b) Pd(PPh_3)$_4$. *iii.* oxalic acid, THF/MeOH (1:1), 50 °C. *iv.* anhydrous $MgCl_2$, paraformaldehyde, NEt_3, CH_3CN, reflux. *v.* 3,3′-diaminodiphenylsulfone, trifluoroacetic acid, dry CH_3CN.

Assembly of Diiron(II) Complexes. The phenolate-to-iron charge-transfer band is a useful spectroscopic probe for quantitating metal−ligand binding.[40,53,54] A previous study demonstrated that the non-macrocyclic syn *N*-donors L^{2-} and BIPS^{2-}, the doubly deprotonated forms of $H_2L^{Me,Ph}$ and H_2BIPS (Chart 1), respectively, react with iron in a 1:1 ratio to form [Fe_2(syn *N*-donor)$_2$] species. To test whether PIM^{2-} exhibits different metal binding behavior, iron(II) titration experiments were conducted. When H_2PIM was treated with 2 equiv of sodium hexamethyldisilazide (NaHMDS) in tetrahydrofuran, optical bands at 240, 280, and 420 nm appeared, corresponding to formation of PIM^{2-}. Addition of iron(II) triflate to the PIM^{2-} solution decreased the intensity of the 240 and 420 nm bands, with concomitant absorption increases at 280 and 375 nm (SI, Figure S1A). A plot of the absorbance changes at 375 nm revealed an Fe-to-PIM^{2-} ratio of 2:1 (Figure S1B), consistent with binding of two iron atoms by each macrocycle to give [Fe_2(PIM)(SO_3CF_3)$_2$]. To examine further the nature of this diiron species, titration experiments were conducted using external carboxylates. Addition of sodium triphenylacetate to a solution containing [Fe_2(PIM)(SO_3CF_3)$_2$] generated new absorption features at 410 and 600 nm (Figure S1C). A plot of the absorbance changes at 410 nm indicated that carboxylates readily displace the triflate anions (Figure S1D).

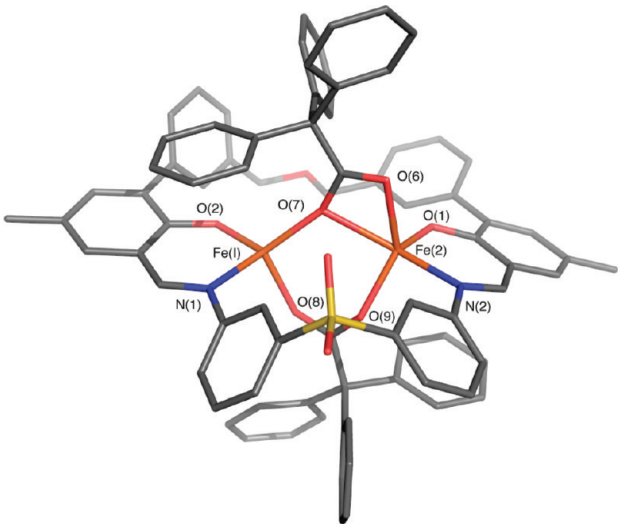

Figure 1. Stick figure representation of the X-ray crystal structure of $[Fe_2(PIM)(Ph_3CCO_2)_2]$ (**1**). Solvent molecules and hydrogen atoms are omitted for clarity. Color scheme: iron, orange; carbon, gray; nitrogen, blue; oxygen, red; sulfur, yellow. Selected bond distances (Å) and angles (deg): Fe(1)−Fe(2) = 3.6100(6); Fe(1)−N(1) = 2.049(2); Fe(1)−O(2) = 1.878(2); Fe(1)−O(7) = 1.999(2); Fe(1)−O(8) = 2.016(2); Fe(2)−N(2) = 2.039(2); Fe(2)−O(1) = 1.892(2); Fe(2)−O(7) = 2.254(2); Fe(2)−O(6) = 2.153(2); Fe(2)−O(9) = 2.024(2); O(2)−Fe(1)−N(1) = 92.49(8); O(1)−Fe(2)−N(2) = 92.38(8); O(7)−Fe(1)−O(8) = 103.72(8); O(7)−Fe(2)−O(9) = 89.14(7). A thermal ellipsoid ORTEP diagram of **1** is provided in SI Figure S13.

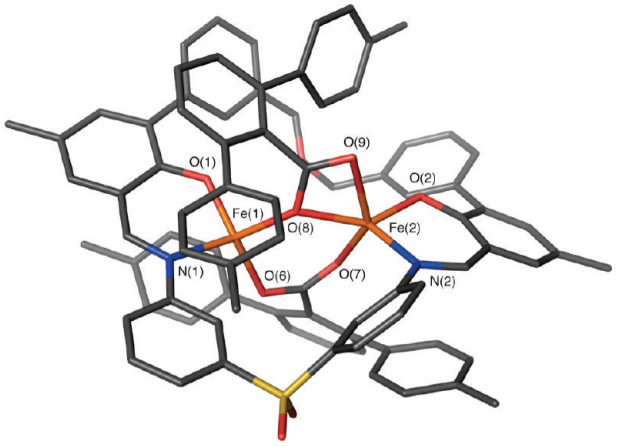

Figure 2. Stick figure representation of the X-ray crystal structure of $[Fe_2(PIM)(Ar^{Tol}CO_2)_2]$ (**2**). Solvent molecules and hydrogen atoms are omitted for clarity. Color scheme: iron, orange; carbon, gray; nitrogen, blue; oxygen, red; sulfur, yellow. Selected bond distances (Å) and angles (deg): Fe(1)−Fe(2) = 3.607(1); Fe(1)−O(1) = 1.888(4); Fe(1)−N(1) = 2.037(4); Fe(1)−O(6) = 1.998(3); Fe(1)−O(8) = 2.028(3); Fe(2)−O(2) = 1.894(3); Fe(2)−N(2) = 2.045(4); Fe(2)−O(7) = 2.048(4); Fe(2)−O(8) = 2.092(3); Fe(2)−O(9) = 2.342(4); O(1)−Fe(1)−N(1) = 93.1(2); O(2)−Fe(2)−N(2) = 91.8(2); O(6)−Fe(1)−O(8) = 102.1(1); O(7)−Fe(2)−O(8) = 89.5(1). A thermal ellipsoid ORTEP diagram of **2** is provided in SI Figure S14.

These data suggested that H_2PIM supports a diiron(II) structure with carboxylate ligands.

Preparative-scale reactions were performed to metalate H_2PIM by treatment with $[Fe_2(Mes)_4]$ and a sterically hindered

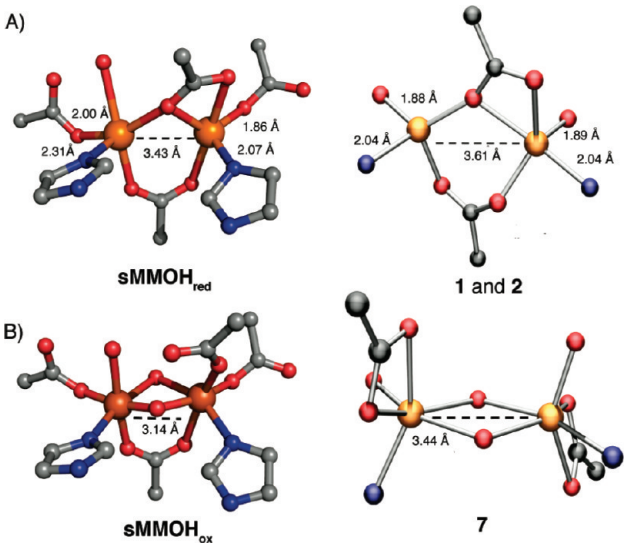

Figure 3. Depiction of the X-ray crystal structures of the diiron sites of $sMMOH_{red}$ (top, left) and $sMMOH_{ox}$ (bottom, left). For structural comparison, the synthetic complexes that mimic each protein state are shown on its right. Some relevant bond lengths are provided; the distances shown for **1** and **2** are averaged over the two complexes. Color scheme: iron, orange; nitrogen, blue; oxygen, red; carbon, gray.

carboxylic acid, triphenylacetic acid or terphenylcarboxylic acid. A diiron(II) unit containing triphenylacetate was crystallized by slow diffusion of pentane into a solution of the compound in benzene. X-ray diffraction studies revealed a dinuclear complex having the molecular formula $[Fe_2(PIM)(Ph_3CCO_2)_2]$ (**1**, Figure 1, SI Table S1). The PIM^{2-} ligand coordinates to two iron atoms that are bridged by two triphenylacetates, one of which is bound in an η^1,η^1-1,3 coordination mode and the other in an η^1,η^2-1,3 arrangement. The Fe−O(carboxylate) distances range from 2.00 to 2.25 Å. The four- and five-coordinate iron atoms are separated by 3.61 Å, with average Fe−O(phenolate) and Fe−N(imine) distances of 1.88 and 2.04 Å, respectively.

When the terphenylcarboxylate anion $Ar^{Tol}CO_2^-$ was employed in an analogous synthetic procedure, crystallization by slow diffusion of pentane into a saturated dichloromethane solution of the compound yielded $[Fe_2(PIM)(Ar^{Tol}CO_2)_2]$ (**2**, Figure 2, Table S1). The X-ray diffraction analysis shows that the dinuclear core in **2** closely resembles that in **1**. The iron atoms in **2** are bridged by two terphenylcarboxylate ligands, with Fe−O(carboxylate) distances of 2.00−2.34 Å. This diiron unit is supported by the syn *N*-donor macrocycle, resulting in Fe−O(phenolate) and Fe−N(imine) distances of 1.89 and 2.04 Å, respectively. The Fe−Fe distance in **2** is 3.61 Å, the same as in **1**.

To a first approximation, the structural parameters of the primary coordination spheres of **1** and **2** compare favorably to those of the diiron core in $sMMOH_{red}$ (Figure 3). The most notable difference is in the Fe−Fe bond distance, 3.43 Å in the protein and 3.61 Å in the model compounds. Differences in metal−metal distance can arise from several factors, such as the donor strength of supporting ligands, constraints of the ligand backbone, and orientation of the bridging carboxylates.

Compounds **1** and **2** were further characterized by several spectroscopic methods (Table 1). As shown in Figure 4, they have strong absorption bands in the UV−visible region, with λ_{max} values of approximately 290 and 410 nm. The higher energy band is attributed to a $\pi-\pi^*$ ligand transition, whereas the lower

Table 1. Characterization Data for 1−8

	optical[a]	Mössbauer[b]								X-ray
	λ, nm [ε, M^{-1} cm^{-1}]	δ(Fe1) [mm/s]	ΔE_Q(Fe1) [mm/s]	Γ(Fe1) [mm/s]	Area(Fe1) [%]	δ(Fe2) [mm/s]	ΔE_Q(Fe2) [mm/s]	Γ(Fe2) [mm/s]	Area(Fe2) [%]	Fe−Fe (Å)
1	290 (36 300)	1.18	2.33	0.38	53	0.97	2.25	0.35	47	3.61
	410 (16 000)									
2	290 (36 700)	1.10	2.04	0.38	63	0.95	2.02	0.32	37	3.61
	418 (14 000)	1.23*	2.58*	0.57*	59*	1.15*	1.75*	0.49*	41*	
3	290 (32 300)	0.49*	1.38*	0.56*	100*	—	—	—	—	3.01
	375(11 100)									
	479 (3300, sh)									
	600 (2300)									
4	284 (108 000)	0.52	0.95	0.38	100	—	—	—	—	3.49
	372 (38 000)									
	570 (10 300)									
5	370 (25 000)	0.51	1.06	0.40	100	—	—	—	—	3.06
	540 (8060)									3.78[c]
6/7	380 (sh)	0.47	1.52	0.36	21	0.50	0.97	0.48	79	3.44
	473	0.46[d]	1.59[d]	0.58[d]	85[d]	0.48[d]	1.03[d]	0.34[d]	15[d]	
	600	0.51*	1.24*	0.62*	61*	0.49*	0.78*	0.44*	36*	
8	360 (81 700)	0.49*	0.97*	0.44*	100*	—	—	—	—	—
	550 (17 100)									

[a] Absorption spectra were recorded in dichloromethane. [b] Mössbauer spectra were acquired at 80 K. Polycrystalline samples were prepared by mixing with Apiezon M grease, and solution samples, which are marked with an asterisk (*), were prepared in tetrahydrofuran. [c] This value corresponds to the Fe−Fe distance between two diiron units. [d] The polycrystalline sample of **6/7** was dried under vacuum at 150 °C for 24 h.

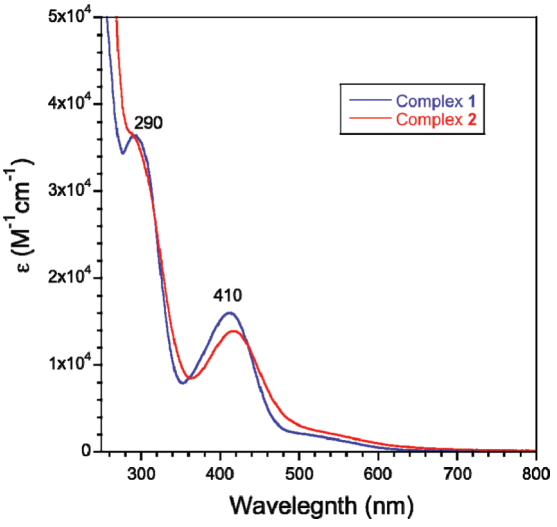

Figure 4. Absorption spectra of **1** and **2** in dichloromethane. Both compounds exhibit optical bands at ~290 and 410 nm.

energy band is most likely due to ligand-to-metal charge transfer.[55,56] In addition, there is a pronounced shoulder at ~540 nm.

The zero-field Mössbauer spectrum of polycrystalline **1** at 80 K displays two quadrupole doublets, with parameters δ_1 = 1.18(2) mm/s, ΔE_{Q1} = 2.33(2) mm/s, δ_2 = 0.97(2) mm/s, and ΔE_{Q2} = 2.25(2) mm/s (Figure 5, Table 1). Each iron site accounts for ~50% of the total iron content in the sample.[57] The Mössbauer spectrum of polycrystalline **2** recorded at 80 K also contains two quadrupole doublets, which were fit with parameters δ_1 = 1.10(2) mm/s, ΔE_{Q1} = 2.04(2) mm/s, δ_2 = 0.95(2) mm/s, and ΔE_{Q2} = 2.02(2) mm/s (Table 1). The isomer shift values of **1** and **2** ($\geq$~1.0 mm/s) are typical of high-spin iron(II) complexes, and the quadruople splitting parameters are as expected for iron coordinated by *O,N*-donors.[30,58] A comparison of the Mössbauer parameters of **1** and **2** to those reported for $sMMOH_{red}$ indicates that there are relatively minor electronic differences between the synthetic and biological complexes. Although the X-ray structure of $sMMOH_{red}$ revealed a diiron core with two different iron environments, the Mössbauer data were fit to a single-quadrupole doublet (δ_1 = 1.3 mm/s, ΔE_{Q1} = 3.0 mm/s).[59] The primary difference between **1** and **2** compared to $sMMOH_{red}$ is the identity of several donor groups, phenolates in place of carboxylates and imines in place of imidazoles. By modifying the electronic properties of the PIM^{2-} or carboxylate ligands in **1** and **2**, however, a better match of the Mössbauer parameters to those of the biological cofactor may be achieved.

To further evaluate the electronic structure, an EPR spectrum of **1** in 2-methyltetrahydrofuran was recorded at 5 K (SI Figure S3). The spectrum exhibits a broad signal with $g \approx 15$, similar to that recorded for $sMMOH_{red}$, in which two $S = 2$ iron(II) centers are weakly ferromagnetically coupled.[60] Although typically lower than 15, mononuclear high-spin iron(II) compounds can also exhibit high g values,[61,62] but we nonetheless attribute this signal to a diiron(II) species. Compelling evidence for such an assignment comes from (1) iron titration experiments, described in the preceding section, indicating that **1** is dinuclear in solution, and (2) the solid-state structure of **1**, which reveals an Fe−Fe separation short enough to support magnetic exchange coupling. The EPR spectrum of **2** was not measured, but because its

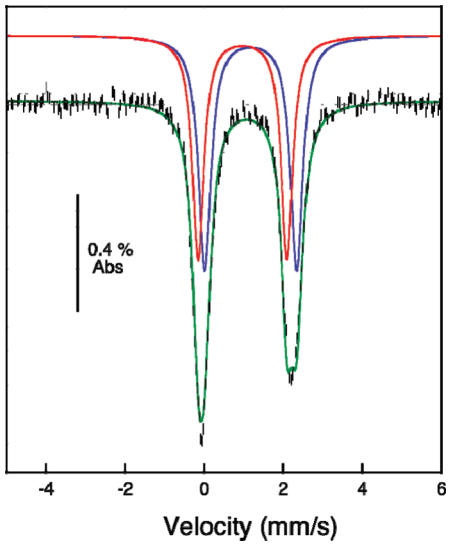

Figure 5. Zero-field ^{57}Fe Mössbauer spectrum of a polycrystalline sample of [Fe_2(PIM)(Ph_3CCO_2)] (**1**) at 80 K. The raw data (black hash lines) were fit to two distinct iron sites (green trace). The single-site fits are shown as blue and red traces using the following parameters: δ_1 = 1.18(2) mm/s, ΔE_{Q1} = 2.33(2) mm/s, $\Gamma_{L/R(1)}$ = 0.38(2) mm/s; δ_2 = 0.97(2) mm/s, ΔE_{Q2} = 2.25(2) mm/s, $\Gamma_{L/R(2)}$ = 0.35(2) mm/s.

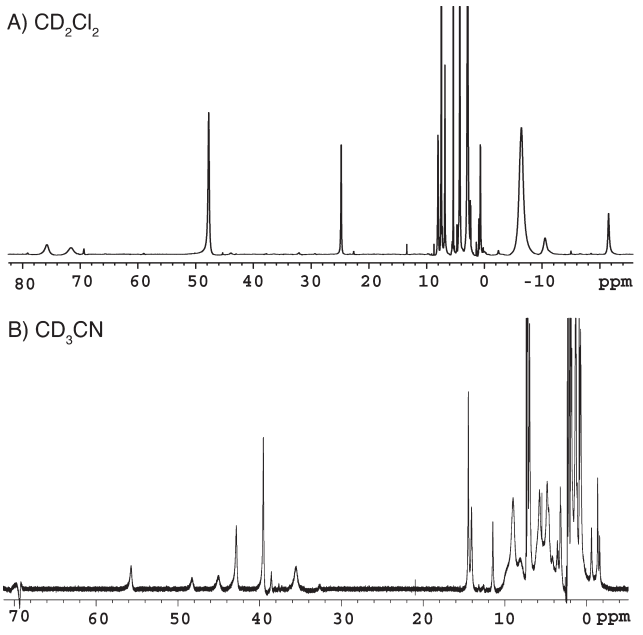

Figure 6. ^{1}H NMR spectra (500 MHz) of ~5 mM [Fe_2(PIM)-($Ar^{Tol}CO_2$)$_2$] (**2**) in solutions of (A) dichloromethane-d_2 and (B) acetonitrile-d_3 at room temperature.

UV−visible and Mössbauer spectra are similar to those of **1**, it most likely shares the same electronic structure.

The paramagnetism of **1** and **2** was verified by NMR spectroscopy. ^{1}H NMR spectra of **1** (SI Figure S2) and **2** (Figure 6A) in dichloromethane-d_2 display resonances ranging from approximately 80 to −20 ppm. Although these paramagnetically shifted resonances cannot be assigned without more detailed studies,[63,64] the peaks at 78.37, 74.97, 48.27, 22.78, −5.32, −10.37, −21.13 ppm for **1** and at 76.92, 73.82, 49.00, 24.68, −5.72, −9.04, −19.60 ppm

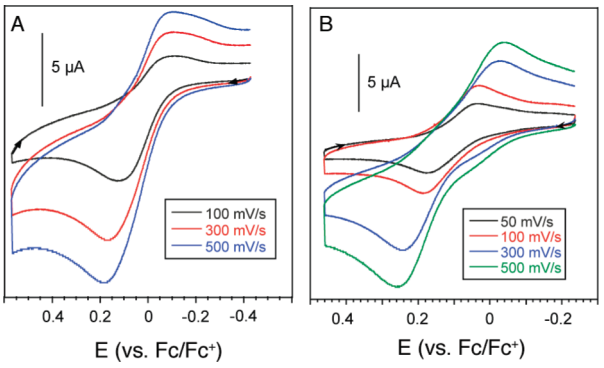

Figure 7. Cyclic voltammograms of 1.0 mM solutions of **1** (A) and **2** (B) in dichloromethane at various scan rates. Tetra-*n*-butylammonium hexafluorophosphate (0.2 M) was used as the supporting electrolyte. All data were obtained using a platinum working electrode, and electrochemical potentials are referenced externally to the ferrocene/ferrocenium couple. Quasi-reversible redox couples at +16 and +108 mV were measured for **1** and **2**, respectively, at a scan rate of 100 mV/s.

for **2** correspond to the PIM^{2-} ligand. Because dichloromethane is a non-coordinating solvent, the solution structures of **1** and **2** in CD_2Cl_2 are probably similar to those in the solid state. When the ^{1}H NMR spectrum of **2** was recorded in acetonitrile-d_3 (Figure 6B), significant shifts in the proton peaks were observed by comparison to the spectrum acquired in dichloromethane-d_2. Most notably, new resonances at 69.33, 55.70, 48.28, 45.03, 42.85, 39.54, 38.55, and 35.55 ppm were present. Because acetonitrile is coordinating, it is possible that solvent molecules bind to the iron centers and/or displace the carboxylate ligands. These data suggest that the solution structures of **1** and **2** depend on the coordinating abilities of the solvent.

Redox Chemistry of Diiron(II) Complexes. A characteristic property of carboxylate-bridged diiron proteins is their tendency to undergo single-electron-transfer reactions.[60] For example, treatment of $sMMOH_{ox}$, which contains a diiron(III) unit, with sodium dithionite or γ radiation from a Co-60 source led to formation of a mixed-valent diiron(II,III) species (H_{mv}). Because **1** and **2** are close structural models of $sMMOH_{red}$, their electrochemical properties are of interest.

A cyclic voltammogram (CV) of **1** measured in dichloromethane using a platinum working electrode and (n-Bu_4N)PF_6 as supporting electrolyte revealed two electrochemical events (Figure 7A and SI Figure S4A). At a scan rate of 100 mV/s, a quasi-reversible redox couple at +16 mV, with a relatively large peak-to-peak separation of +210 mV, and an irreversible oxidation at +840 mV were observed. The CV of **2** was recorded under identical conditions (Figures 7B and S4B) and displayed a similar voltammogram, showing a quasi-reversible oxidation at +108 mV (ΔE_p = +198 mV) and an irreversible oxidation at +600 mV. It is uncertain whether the quasi-reversible waves involve a one- or two-electron process and whether the large peak-to-peak separation is due to structural reorganization or some other chemical process. Ligand-centered redox chemistry, observed in some phenolate iron complexes,[65−67] is also a possibility that cannot be ruled out at this time.

The redox chemistry of complex **2** was further explored by using chemical oxidants (Scheme 3). Because the Ag^+/Ag^0 redox couple has an $E_{1/2}$ value of +650 mV (vs ferrocene/ferrocenium) in dichloromethane,[68] silver(I) reagents were expected to oxidize **2** ($E_{1/2}$ = +108 mV). Treatment of **2** with ~1 equiv of $AgClO_4$ in

Scheme 3. Summary of Reaction Products Characterized in This Study[a]

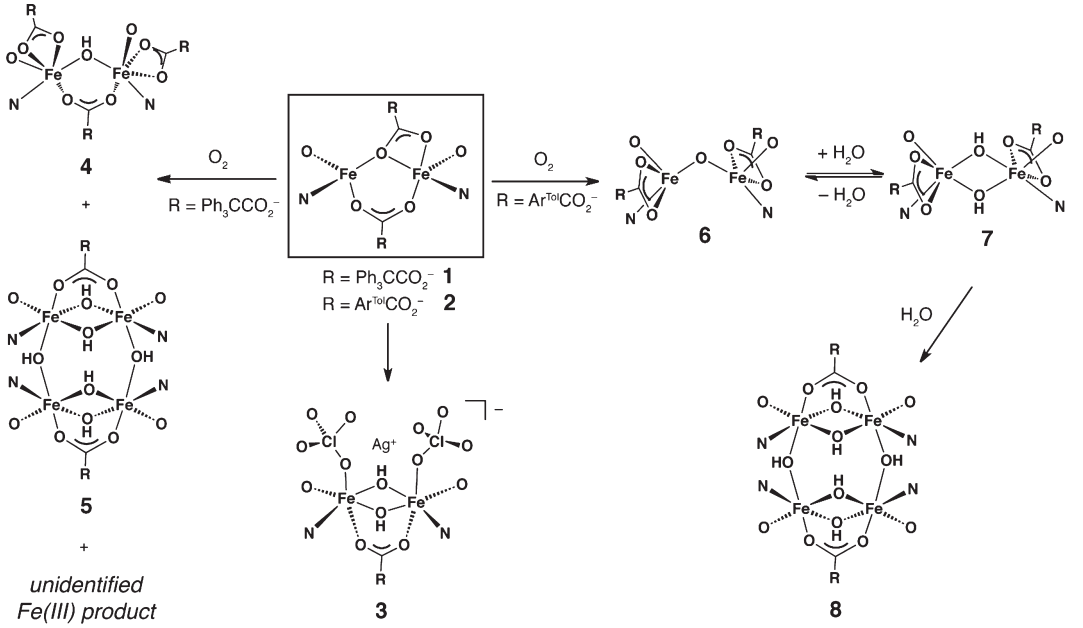

[a] Full representation of the PIM^{2-} ligand is omitted for clarity; only its phenolate oxygen and imine nitrogen atoms are depicted. See Chart 1 for the structure of H_2PIM, the doubly protonated form of PIM^{2-}.

dichloromethane gradually converted the initial dark red solution to a pale yellow brown solution. After the solution was stirred for about 1 h, a black precipitate, presumed to be silver metal, formed. This insoluble material was removed by filtration, and the absorption spectrum of the filtrate revealed formation of a new product that exhibited optical bands at 290, 375, 479 (sh), and 600 nm (SI Figure S5). The filtrate was concentrated, and pentane was introduced by diffusion, affording a small number of X-ray diffraction quality crystals. Structural analysis of these crystals revealed the product to be $[Fe_2(\mu\text{-}OH)_2(ClO_4)_2(PIM)(Ar^{Tol}CO_2)Ag]$ (**3**), containing a di(μ-hydroxo)diiron(III) unit and a silver(I) ion. Because the synthesis of **3** was performed under anhydrous anaerobic conditions, the most likely source of the OH^- groups is trace water in the reaction mixture. Using 3.5 equiv of $AgClO_4$, instead of 1.0 equiv, provided a higher yield of **3** (see Experimental Section).

The octahedral iron atoms (Fe−Fe = 3.01 Å) in **3** are bridged by two hydroxide ions ($Fe-O_{ave}$ = 2.02 Å) and one terphenylcarboxylate ligand ($Fe-O_{ave}$ = 2.04 Å) (Figure 8). The hydrogen atoms of the hydroxides were not located, but the protonation state could be confidently assigned on the basis of the Fe−O bond distances. Whereas bridging hydroxides afford Fe−O distances of 1.9−2.1 Å, bridging oxides have Fe−O bond lengths in the 1.7−1.8 Å range.[69,70] The phenolate ($Fe-O_{ave}$ = 1.86 Å) and imine ($Fe-N_{ave}$ = 2.12 Å) donors of PIM^{2-} and a perchlorate anion ($Fe-O_{ave}$ = 2.13 Å) make up the rest of the iron coordination sphere. A silver(I) ion is disordered over two positions within the interior of the macrocycle. Ag(1A) interacts with a hydroxide ligand (Ag−O(6) = 2.25 Å), the ether oxygen of PIM^{2-} (Ag−O(5) = 2.36 Å), and a C=C π bond of the terphenylcarboxylate moiety (Ag−C(60) = 2.49 Å, Ag−C(61) = 2.74 Å). Ag(1B), a minority species, has close contacts with a hydroxide ligand (Ag−O(6) = 2.33 Å), the ether oxygen of PIM^{2-} (Ag−O(5) = 2.40 Å), and one of the aromatic carbon atoms (Ag−C(60) = 2.69 Å) (SI Figure S15). The Ag−C distances are within the 2.36−2.77 Å limit reported for other silver(I)−aryl interactions.[71−73] A bond valence sum (BVS) analysis,[74,75] an empirical quantity used to determine the oxidation state of metal ions in coordination compounds on the basis of crystallographically determined metal−ligand distances, returned values of 3.12 and 3.07 for Fe(1) and Fe(2), respectively (SI Table S2), indicating that the iron centers in **3** are both in the +3 oxidation state.

To provide further evidence for this assignment, the Mössbauer spectrum of a frozen solution of **3** in tetrahydrofuran was recorded at 80 K (Table 1). The data could be satisfactorily fit to a single quadrupole doublet, with δ = 0.49(2) mm/s and ΔE_Q = 1.38(2) mm/s, parameters typical of iron(III) complexes having mixed oxygen and nitrogen donor groups. The single quadrupole doublet in the Mössbauer spectrum is consistent with the X-ray crystal structure of **3**, which has two chemically equivalent iron centers. The reason for the broad line width (Γ = 0.56 mm/s, Table 1) is not immediately clear, but it may be due to the presence of a second closely related diiron(III) species in the sample or slow nuclear relaxation rate of the iron atoms at 80 K.[76]

Because chemical oxidation of **2** using $AgClO_4$ led to metal binding by the perchlorate anion, the oxidation was repeated using the silver salt of a less coordinating anion, $AgSbF_6$. Reaction of **2** with 1 equiv of $AgSbF_6$ in dichloromethane yielded a heterogeneous dark brown solution over the course of ~1 h. After removal of a black solid, the UV−vis spectrum of the filtrate revealed bands at 300, 374, and 605 nm (SI Figure S6), suggesting formation of a new species. Single crystals of the product were grown by slow diffusion of diethyl ether into an acetonitrile solution containing the material. X-ray diffraction studies revealed a tetranuclear complex, $[Fe_4(\mu\text{-}X)_4(\mu\text{-}Y)_2(PIM)_2(Ar^{Tol}CO_2)_2]$, where the identity of atoms X and Y is probably F^-. We have not been able to fully solve this structure owing to unresolved disorder in the crystal. On the basis of its optical spectrum, however, we can rule out $[Fe_4(\mu\text{-}OH)_6(PIM)_2(Ar^{Tol}CO_2)_2]$ (**8**) as a possible product (vide infra).

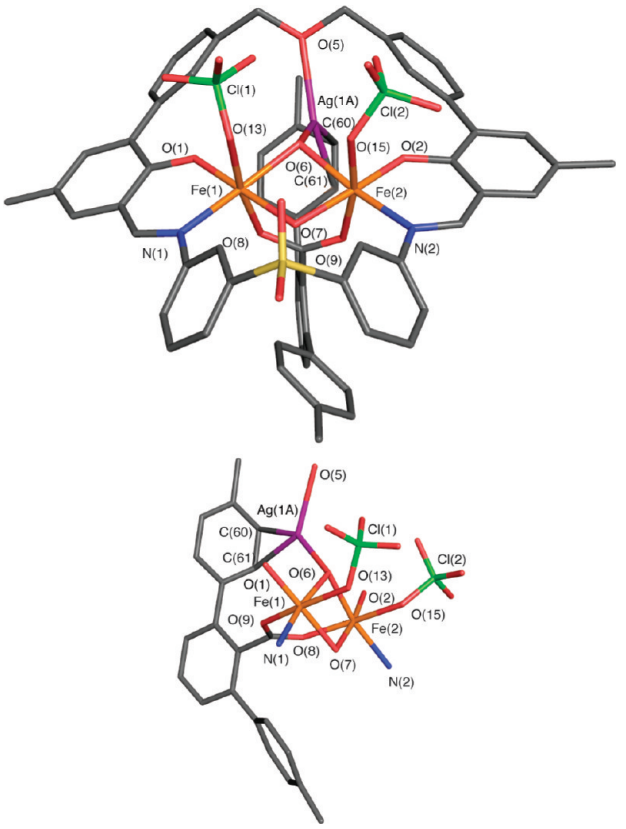

Figure 8. Stick figure representation of the X-ray crystal structure of $[Fe_2(\mu\text{-}OH)_2(ClO_4)_2(PIM)(Ar^{Tol}CO_2)Ag]$ (**3**, top). An isolated view of the heterometallic core is shown in the diagram below. The silver ion is disordered over two positions; the major component (Ag(1A), ~91% occupancy) is depicted. Solvent molecules and hydrogen atoms are omitted for clarity. Color scheme: iron, orange; carbon, gray; nitrogen, blue; oxygen, red; sulfur, yellow; green, chlorine; purple, silver. Selected bond distances (Å) and angles (deg): Fe(1)−Fe(2) = 3.0119(8); Fe(1)−O(1) = 1.847(3); Fe(1)−N(1) = 2.119(4); Fe(1)−O(6) = 2.048(3); Fe(1)−O(7) = 1.996(3); Fe(1)−O(8) = 2.030(3); Fe(1)−O(13) = 2.124(3); Fe(2)−O(2) = 1.866(3); Fe(2)−N(2) = 2.128(4); Fe(2)−O(6) = 2.043(3); Fe(2)−O(7) = 1.974(3); Fe(2)−O(9) = 2.048(3); Fe(2)−O(15) = 2.136(3); Ag(1A)−O(6) = 2.260(3); Ag(1A)−O(5) = 2.414(3); Ag(1A)−C(60) = 2.349(5); Ag(1A)−C(61) = 2.596(5); O(1)−Fe(1)−N(1) = 88.5(1); O(2)−Fe(2)−N(2) = 88.8(1); Fe(1)−O(6)−Fe(2) = 94.8(1); Fe(1)−O(7)−Fe(2) = 98.6(1); O(5)−Ag(1A)−O(6) = 109.5(1); O(5)−Ag(1A)−C(60) = 100.4(1); O(6)−Ag(1A)−C(61) = 117.4(1). See SI Figure S15 for a depiction of Ag(1B): Ag(1B)−O(6) = 2.335(6), Ag(1B)−O(5) = 2.404(6), Ag(1B)−C(60) = 2.687(8), O(5)−Ag(1B)−O(6) = 107.3(2), O(6)−Ag(1B)−C(60) = 124.7(3), O(5)−Ag(1B)−C(60) = 91.7(2). A thermal ellipsoid ORTEP diagram of **3** is provided in Figure S15.

Reactivity with O_2. To determine whether **1** and **2** exhibit the same functional activity as the diiron cores in the BMM proteins,[3] their reactivity with dioxygen was investigated (Scheme 3). Exposure of a dichloromethane solution of **1** to dioxygen at room temperature led to an instantaneous color change and the appearance of new optical bands at 370 and 570 nm (Figure 9, black trace). Facile reactivity of **1** with O_2 was confirmed by NMR spectroscopy. Injecting O_2 into a septum-sealed NMR tube containing **1** in dichloromethane-d_2 afforded the ^{1}H NMR spectrum shown in Figure 10A. The numerous proton resonances in the

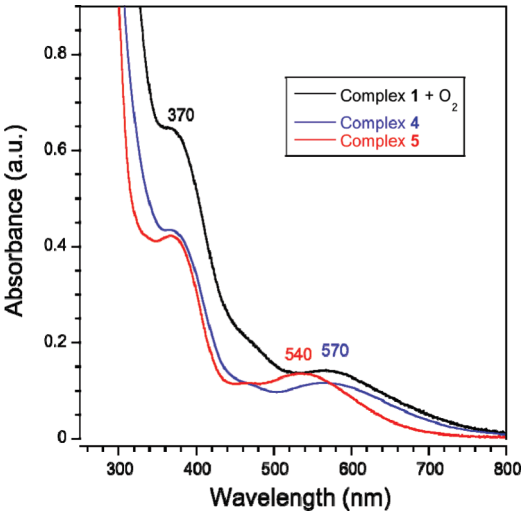

Figure 9. Absorption spectra of **1** + O_2 (black trace), **4** (blue trace), and **5** (red trace) in dichloromethane.

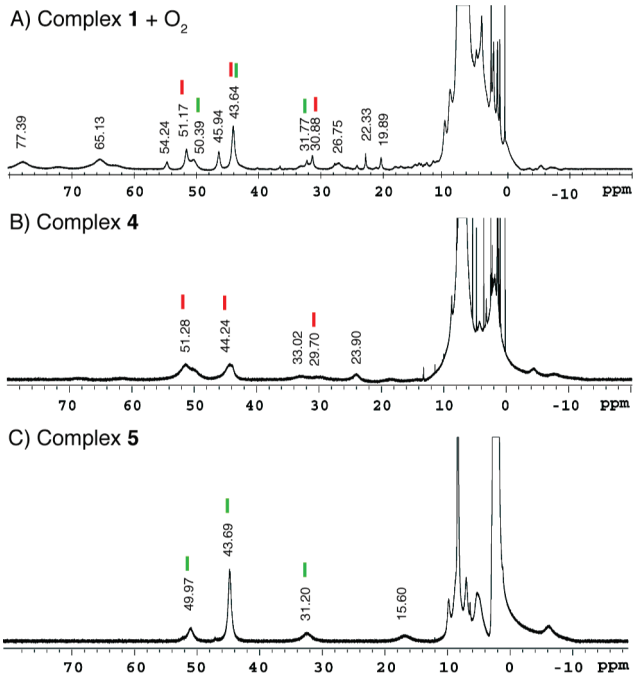

Figure 10. ^{1}H NMR spectra (500 MHz) of (A) $[Fe_2(PIM)(Ph_3CCO_2)_2]$ (**1**) + O_2, (B) $[Fe_2(\mu\text{-}OH)(PIM)(Ph_3CCO_2)_3]$ (**4**), and (C) $[Fe_4(\mu\text{-}OH)_6(PIM)_2(Ph_3CCO_2)_2]$ (**5**). Comparison of spectrum A to spectra B and C reveals that reaction of **1** with O_2 leads to formation of **4** and **5**, in addition to at least one other product. The peaks that most likely arise from **4** and **5** in spectrum A are marked with red and green lines, respectively. Not all of the peaks in A corresponding to **4** and **5** were assigned because of uncertainty due to the broadness and overlap of some resonances. All spectra were recorded at room temperature with diiron complex concentrations of ~5−10 mM in $CDCl_3$. Relative peak heights are *not* normalized between spectra.

spectrum, ranging from approximately 80 to −10 ppm, suggest the formation of multiple species in the reaction mixture.

To characterize the reaction product(s), single crystals of the material were grown by slow diffusion of pentane into a benzene solution containing the dark red-brown solid. After several days, a

dx.doi.org/10.1021/ja2021312 |*J. Am. Chem. Soc.* 2011, 133, 10568–10581

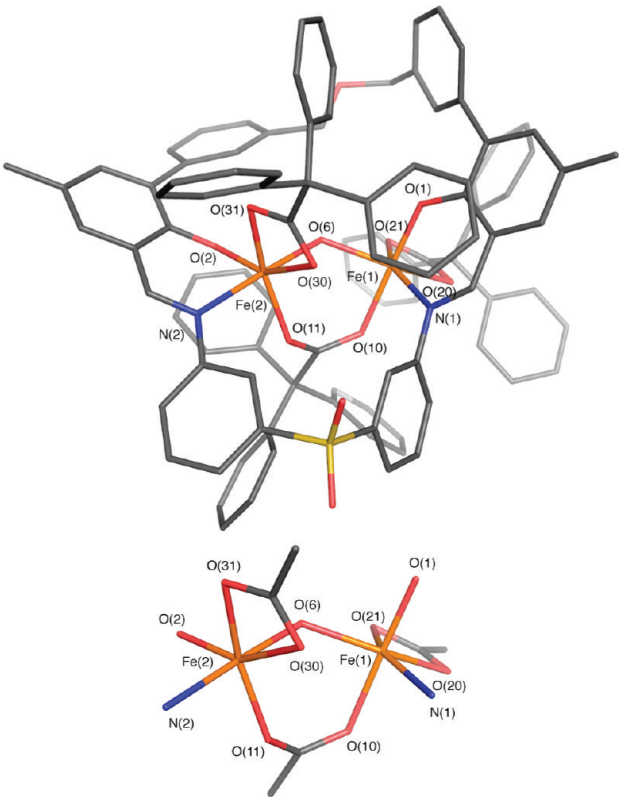

Figure 11. Stick figure representation of the X-ray crystal structure of $[Fe_2(\mu\text{-OH})(PIM)(Ph_3CCO_2)_3]$ (**4**, top). An isolated view of the diiron core is shown in the diagram below. Solvent molecules and hydrogen atoms are omitted for clarity. Color scheme: iron, orange; carbon, gray; nitrogen, blue; oxygen, red; sulfur, yellow. Selected bond distances (Å) and angles (deg): Fe(1)−Fe(2) = 3.4873(5); Fe(1)−O(1) = 1.890(2); Fe(1)−N(1) = 2.115(2); Fe(1)−O(6) = 1.951(2); Fe(1)−O(10) = 2.064(2); Fe(1)−O(20) = 2.075(2); Fe(1)−O(21) = 2.133(2); Fe(2)−O(2) = 1.872(2); Fe(2)−N(2) = 2.136(2); Fe(2)−O(6) = 1.968(2); Fe(2)−O(11) = 1.980(2); Fe(2)−O(30) = 2.141(2); Fe(2)−O(31) = 2.094(2); O(1)−Fe(1)−N(1) = 87.42(7); O(2)−Fe(2)−N(2) = 87.47(7); Fe(1)−O(6)−Fe(2) = 125.69(9); O(6)−Fe(1)−O(10) = 88.28(7); O(6)−Fe(2)−O(11) = 88.89(7). A thermal ellipsoid ORTEP diagram of **4** is provided in SI Figure S16.

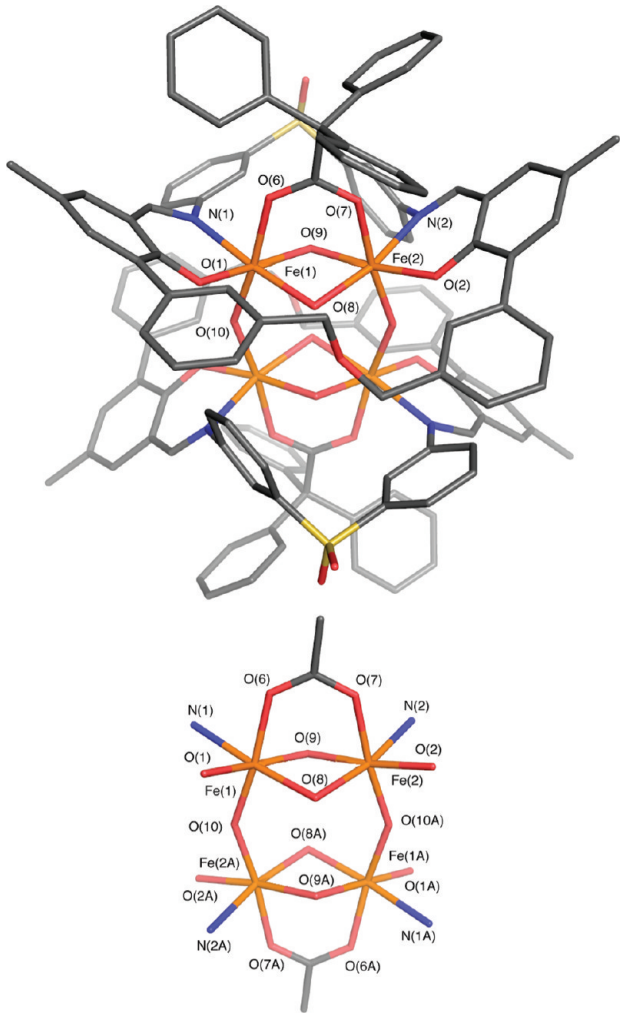

Figure 12. Stick figure representation of the X-ray crystal structure of $[Fe_4(\mu\text{-OH})_6(PIM)_2(Ph_3CCO_2)_2]$ (**5**, top). The center of the complex is located on a crystallographic inversion center. An isolated view of the tetrairon core is depicted in the diagram below. Solvent molecules and hydrogen atoms are omitted for clarity. Color scheme: iron, orange; carbon, gray; nitrogen, blue; oxygen, red; sulfur, yellow. Selected bond distances (Å) and angles (deg): Fe(1)−Fe(2) = 3.0560(5); Fe(1)−Fe(2A) = 3.780 (standard deviation not calculated); Fe(1)−O(1) = 1.912(2); Fe(1)−N(1) = 2.172(2); Fe(1)−O(6) = 2.042(2); Fe(1)−O(8) = 2.030(2); Fe(1)−O(9) = 1.998(2); Fe(1)−O(10) = 1.978(2); Fe(2)−O(2) = 1.910(2); Fe(2)−N(2) = 2.229(2); Fe(2)−O(7) = 2.073(2); Fe(2)−O(8) = 2.029(2); Fe(2)−O(9) = 2.011(2); N(1)−Fe(1)−O(1) = 83.38(8); N(2)−Fe(2)−O(2) = 85.42(8); Fe(1)−O(8)−Fe(2) = 97.70(9); Fe(1)−O(9)−Fe(2) = 99.35(9); Fe(1)−O(10)−Fe(1A) = 146.5(1). A thermal ellipsoid ORETP diagram of **5** is provided in SI Figure S17.

mixture of dark brown rectangular blocks and dark brown hexagonal prisms was obtained in addition to an amorphous solid. X-ray diffraction analysis of the rectangular-shaped crystals showed that the compound has a (μ-hydroxo)diiron(III) core and the molecular formula $[Fe_2(\mu\text{-OH})(PIM)(Ph_3CCO_2)_3]$ (**4**, Figure 11, Table S1). The distorted octahedral iron centers are separated by 3.49 Å, with Fe(1)−O(6) and Fe(2)−O(6) bond lengths of 1.95 and 1.97 Å, respectively. The hydrogen atom on O(6), the bridging hydroxide ion, was located from a difference Fourier map. The diiron core is supported by the PIM^{2-} ligand, with average Fe−O(phenoxyl) and Fe−N(imine) distances of 1.31 and 2.12 Å, respectively, and three triphenylacetate groups. Two of the carboxylates coordinate to the iron atoms in a terminal bidentate mode, giving average Fe−O distances of 2.11 Å, and the remaining carboxylate bridges the diiron core, with an average Fe−O bond length of 2.02 Å.

X-ray diffraction studies of the hexagonal prisms, isolated from the $\mathbf{1}/O_2$ reaction mixture, revealed a tetranuclear $[Fe_4(\mu\text{-OH})_6(PIM)_2(Ph_3CCO_2)_2]$ complex (**5**), in which two di(μ-hydroxo)(μ-triphenylacetato)diiron(III) units are linked by two bridging hydroxide ions (Figure 12, Table S1). The tetrairon(III) unit is located on a crystallographic inversion center. The diiron subunit bound by the PIM^{2-} ligand has an Fe−Fe distance of 3.06 Å and is bridged by two hydroxide ligands ($Fe-O_{ave}$ = 2.02 Å). The separation of iron atoms between two $[Fe_2PIM]$ monomers is 3.78 Å, and the linkage involves only one hydroxo bridge ($Fe-O_{ave}$ = 1.98 Å). The average Fe−O(phenoxyl) and Fe−N(imine) bond lengths were refined to be approximately 1.91 and 2.20 Å, respectively. Finally, two bridging

dx.doi.org/10.1021/ja2021312 |J. Am. Chem. Soc. 2011, 133, 10568–10581

carboxylate groups (Fe−O_{ave} = 2.06 Å) cap the tetranuclear cluster at opposite ends.

Analytically pure samples of **4** and **5** were prepared for spectroscopic characterization. The dinuclear compound **4** was synthesized by combining triphenylacetic acid, triethylamine, and **1** in benzene, followed by exposure to dioxygen. Vapor diffusion of pentane into the benzene reaction solution over the course of ~24 h afforded dark brown crystals. X-ray diffraction analysis of these crystals confirmed the desired (μ-hydroxo)diiron(III) species **4**. The UV−visible spectrum of **4** exhibits absorption bands at 370 and 570 nm (Figure 9, blue trace). The higher energy band is most likely a ligand $\pi-\pi^*$ transition, whereas the visible band is most likely a hydroxo-to-iron(III) charge transfer.[70] The ^{1}H NMR spectrum of **4** was recorded in chloroform-d_1 (Figure 10B). As expected for a paramagnetic compound, the spectrum shows several broad resonances, ranging from approximately 70 to −10 ppm. Assignment of the metal oxidation states in **4** as iron(III) is supported by zero-field Mössbauer spectroscopic measurements. Polycrystalline ^{57}Fe-enriched **4** displays a single quadrupole doublet in the Mössbauer spectrum, with parameters of δ = 0.52(2) mm/s and ΔE_Q = 0.95(2) mm/s (SI Figure S9A, Table 1). Although the two iron atoms in **4** are not chemically equivalent, similarities in their coordination geometry and donor groups make them indistinguishable by zero-field Mössbauer spectroscopy.

The tetrairon(III) complex **5** was also fully characterized. The compound was isolated as brown crystals by slow evaporation of a benzene solution containing **1** and dioxygen under ambient conditions. To ensure that the bulk product did not contain **4**, several representative crystals were analyzed by X-ray crystallography. In all cases, tetranuclear **5** was obtained. The absorption spectrum has peaks with λ_{max} at 370 and 540 nm (Figure 9, red trace). The visible band, which is blue-shifted by approximately 30 nm from the 570 nm absorption feature in **4**, is most likely a ligand-to-metal transition involving the diiron−hydroxo unit.[70] The ^{1}H NMR spectrum of **5** in chloroform-d_1 exhibits paramagnetically broadened peaks at ~50, 44, 31, 15, and −8 ppm (Figure 10C). The simpler ^{1}H NMR spectrum of **5**, compared to that of **4**, is consistent with its higher molecular symmetry (pseudo-C_{2h} for **5** versus C_1 for **4**). The zero-field Mössbauer spectrum of ^{57}Fe-enriched **5** was fit with parameters that are distinct from those of **4**, giving δ = 0.51(2) mm/s and ΔE_Q = 1.06(2) mm/s (Figure S9B, Table 1). Because the four iron sites in **5** are chemically equivalent, the single-quadrupole doublet observed in the Mössbauer spectrum is consistent with its X-ray structure.

Comparison of the ^{1}H NMR spectrum of **1**/O_2 (Figure 10A) with the spectra of **4** (Figure 10B) and **5** (Figure 10C) reveals that not all of the peaks are accounted for, particularly the broad resonances at ~77, 65, 54, 27, 22, and 20 ppm. To determine the number of iron-containing species generated upon reaction of **1** with dioxygen, the crude **1**/O_2 solid was examined by Mössbauer spectroscopy (SI Figure S8). The Mössbauer data display three overlapping quadrupole doublets, with the following characteristics: δ_1 = 0.50(2) mm/s, ΔE_{Q1} = 0.78(2) mm/s, Area 1 = 24%; δ_2 = 0.51(2) mm/s, ΔE_{Q2} = 1.12(2) mm/s, Area 2 = 37%; δ_3 = 0.52(2) mm/s, ΔE_{Q3} = 1.59(2) mm/s, Area 3 = 39%. The three sites have nearly identical isomer shift values but differ in their quadrupole splitting parameters. On the basis of their similarities to the Mössbauer parameters of the crystallographically characterized species, sites 1 and 2 are ascribed to compounds **4** and **5**, respectively. The nature of the third site, which comprises about 39% of total iron in the **1**/O_2 sample, has not yet been determined.

The dioxygen reactivity of the diiron(II) compound **2**, which contains sterically demanding terphenylcarboxylates rather than triphenylacetates, was also examined (Scheme 3). Exposing a dichloromethane solution of **2** to O_2 led to an immediate color change from bright red to dark brown. The absorption spectrum of dioxygen-treated **2** has features at approximately 380, 473, and 600 nm (SI Figure S10, blue trace). The ^{1}H NMR spectrum revealed new resonances between 26 and −8 ppm (SI Figure S11). Unlike the ^{1}H NMR spectrum of **1**/O_2 (Figure 10A), which shows multiple chemical species in solution, the data suggest that reaction of **2** with O_2 forms fewer products.

To determine the composition of the **2**/O_2 product, preparative-scale reactions were performed to obtain sufficient material for characterization. Single crystals of oxygenated **2** were grown by slow diffusion of diethyl ether into a solution of the complex in acetonitrile. An X-ray structural investigation revealed that each single crystal contains a mixture of two species, a (μ-oxo)diiron(III) [Fe_2(μ-O)(PIM)($Ar^{Tol}CO_2$)$_2$] (**6**) compound and a di(μ-hydroxo)diiron(III) [Fe_2(OH)$_2$(PIM)($Ar^{Tol}CO_2$)$_2$] (**7**) compound (Figure 13, Table S1). This result was verified by analyzing several crystals that were independently prepared by the same method. The structures of **6** and **7** are identical except for the nature of their bridging oxygen atoms, which were modeled with positional disorder and partial occupancies assigned to atoms O(6) [in **6**] and O(100)/O(101) [in **7**]. Data refinement converged with **6** having an occupancy of 76% and **7** of 24%. The iron atoms in both structures are separated by 3.44 Å. Complex **6** is designated as a (μ-oxo)diiron(III) species because of its short Fe(1)−O(6) and Fe(2)−O(6) distances of 1.74 and 1.75 Å, respectively.[70] In contrast, **7** is a di(μ-hydroxo)diiron(III) complex with the longer Fe−O(100) and Fe−O(101) bond length of 2.10 Å (averaged), more typical of a dinuclear structure with bridging hydroxide ligands. The iron atoms of **6** and **7** are coordinated by the PIM^{2-} ligand, with average Fe−O(phenoxyl) distances of 1.89 Å and average Fe−N(imine) distances of 2.11 Å. Furthermore, each iron site contains a terminal terphenylcarboxylate (Fe−O_{ave} = 2.11 Å). The iron atoms in **6** and **7** have bond valence sums of 3.0 and 2.8, respectively (SI Table S2), indicating that the iron centers are in the +3 oxidation state. Although three triphenylacetate ligands are accommodated by the PIM^{2-} platform in **4** (Figure 14A), only two terphenylcarboxylates could occupy the same space in **6** (Figure 14B). These observations underscore the importance of considering both shape and size when selecting an appropriate carboxylate for synthetic modeling studies; a fan-shaped terphenylcarboxylate is preferable over the cone-shaped triphenylacetate for producing dinuclear oxygenated products using the PIM^{2-} ligand framework.

The structure of **7** closely mimics that of the oxidized core of $sMMOH_{ox}$,[11] which also contains a di(μ-hydroxo)diiron(III) unit (Figure 3). We attribute the longer Fe−Fe distance in **7**, compared to $sMMOH_{ox}$, to the lack of a bridging carboxylate. More importantly, however, switching of a bridging $Ar^{Tol}CO_2^-$ in **2** to a terminal position in **7** reproduces the redox-dependent *carboxylate shift* observed in the BMM proteins.[29]

The presence of both (μ-oxo)diiron(III) and di(μ-hydroxo)diiron(III) species in the reaction product of **2** with dioxygen was further supported by zero-field Mössbauer measurements. Polycrystalline **2**/O_2 gave a Mössbauer spectrum that was best fit to two quadrupole doublets, δ_1 = 0.47(2) mm/s, ΔE_{Q1} = 1.52(2) mm/s, δ_2 = 0.50(2) mm/s, and ΔE_{Q2} = 0.97(2) mm/s.

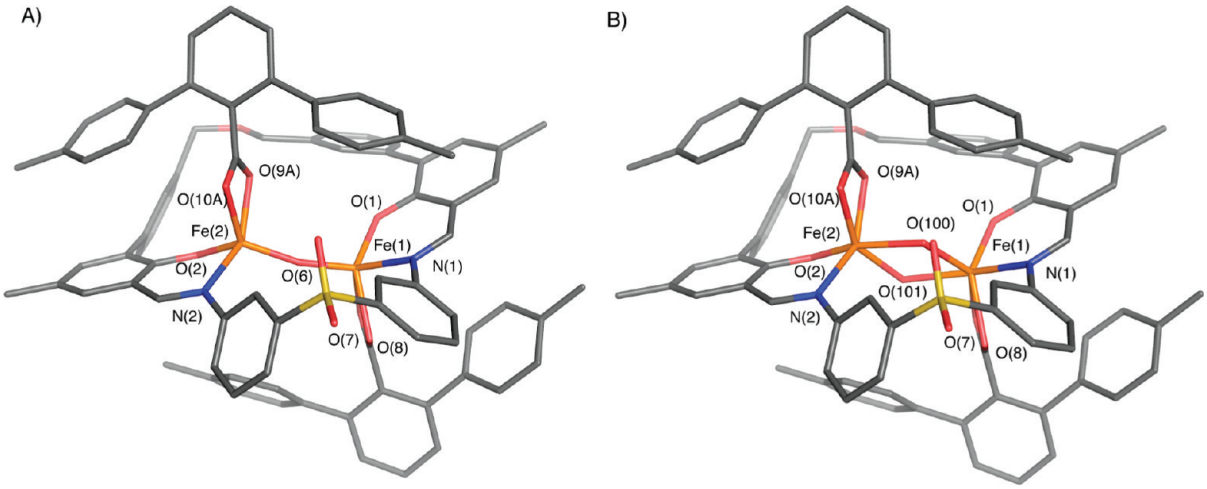

Figure 13. Stick figure representation of the X-ray crystal structure of $[Fe_2(\mu\text{-O})(PIM)(Ar^{Tol}CO_2)_2]$ (**6**, A) and $[Fe_2(\mu\text{-OH})_2(PIM)(Ar^{Tol}CO_2)_2]$ (**7**, B) . The two complexes occur in a single crystal and differ only in their (μ-oxo)diiron(III) and di(μ-hydroxo)diiron(III) cores, respectively. The ratio of **6**:**7** was determined to be 76:24 and is similar in two other independently prepared crystals. Solvent molecules and hydrogen atoms are omitted for clarity. Color scheme: iron, orange; carbon, gray; nitrogen, blue; oxygen, red; sulfur, yellow. Selected bond distances (Å) and angles (deg): Fe(1)−Fe(2) = 3.436(1); Fe(1)−O(1) = 1.880(4); Fe(1)−N(1) = 2.103(5); Fe(1)−O(6) = 1.745(5); Fe(1)−O(7) = 2.086(4); Fe(1)−O(8) = 2.133(4); Fe(1)−O(100) = 2.12(2); Fe(1)−O(101) = 2.09(2); Fe(2)−O(2) = 1.896(4); Fe(2)−N(2) = 2.122(5); Fe(2)−O(6) = 1.751(5); Fe(2)−O(9A) = 2.05(2); Fe(2)−O(10A) = 2.03(2); Fe(2)−O(100) = 2.10(2); Fe(2)−O(101) = 2.08(2); O(1)−Fe(1)−N(1) = 87.1(2); O(2)−Fe(2)−N(2) = 87.9(2); Fe(1)−O(6)−Fe(2) = 158.8(3); Fe(1)−O(100)−Fe(2) = 109.0(9); Fe(1)−O(101)−Fe(2) = 111.0(1). A thermal ellipsoid ORTEP diagram of **6**/**7** is provided in SI Figure S18.

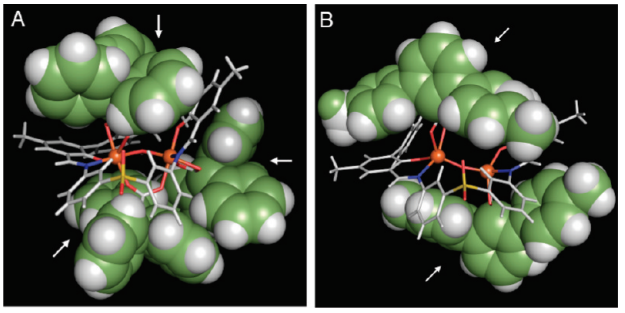

Figure 14. Hybid stick and space-filling diagrams of $[Fe_2(\mu\text{-OH})(PIM)(Ph_3CCO_2)_3]$ (**4**, A) and $[Fe_2(\mu\text{-O})(PIM)(Ar^{Tol}CO_2)_2]$ (**6**, B). The aromatic rings of the carboxylate ligands are representated as spheres (carbon = green, hydrogen = white) to emphasize their shape and volume. The location of the carboxylate unit, either $Ph_3CCO_2^-$ or $Ar^{Tol}CO_2^-$, is indicated by a white arrow. The PIM^{2-} framework is displayed in stick form (carbon/hydrogen, gray; nitrogen, blue; oxygen, red; sulfur, yellow) with the iron atoms shown as orange spheres.

Sites 1 and 2 were refined with areas of 21% and 79%, respectively. Because (μ-oxo)diiron(III) species typically have larger ΔE_Q values (>1.0 mm/s) than (μ-hydroxo)diiron(III) complexes (<1.0 mm/s), site 1 is attributed to complex **6** and site 2 to complex **7**. When the **2**/O_2 solid reaction product was dried under vacuum at 150 °C for 24 h, Mössbauer measurements yielded a **6**:**7** ratio of 85:15 (Table 1), which is similar to the **6**:**7** ratio of 76:24 determined by X-ray crystallography (Figure 13), suggesting that **6** can be obtained from **7** by extrusion of H_2O. To examine the **6**:**7** ratio in solution, an ^{57}Fe-enriched sample of the **2**/O_2 solid dissolved in tetrahydrofuran was studied by Mössbauer spectroscopy at 80 K, yielding the following parameters: $\delta_1 = 0.51(2)$ mm/s, $\Delta E_{Q1} = 1.24(2)$ mm/s, $\delta_2 = 0.49(2)$ mm/s, and $\Delta E_{Q2} = 0.78(2)$ mm/s, with sites 1 and 2 having occupancies of 61% and 36%, respectively (SI Figure S12B). Because site 1 has a larger ΔE_Q value than site 2, the ratio for **6**:**7** in tetrahydrofuran is 61:36. The varying percentages of **6** and **7**, as determined from X-ray crystallographic and Mössbauer spectroscopic measurements, are probably due to the different amounts of H_2O present in each **2**/O_2 sample. Complex **6** probably forms directly from reaction of **2** with dioxygen and converts to **7** by subsequent reaction with water (Scheme 3). Such interconversion between (μ-oxo)dimetallic and di(μ-hydroxo)dimetallic units has been previously observed. Mössbauer spectroscopic studies revealed that drying of a $[Fe^{III}_2(\mu\text{-OH})_2]$ complex resulted in extrusion of water to give a $[Fe^{III}_2(\mu\text{-O})]$ species.[77] More recently, crystal-to-crystal conversion of a (μ-oxo)divanadium polyoxometalate cluster to a di(μ-hydroxo)divandium analogue was discovered following exposure of the starting complex to water vapor.[78] These studies suggest that similar processes may occur in the active sites of non-heme diiron proteins as well.

Because **7** differs from **6** by a single water molecule, we explored whether addition of H_2O could convert the (μ-oxo)diiron(III) species **6** to the di(μ-hydroxo)diiron(III) complex **7**. When a dichloromethane solution of **6**/**7** was treated with 10 μL of H_2O, ~15 equiv relative to the diiron complexes, the brown solution instantaneously turned pale red. New optical bands at 360 and 550 nm were observed (Figure S10, red trace), which are reminiscent of those displayed by the tetrairon complex $[Fe_4(\mu\text{-OH})_6(PIM)_2(Ph_3CCO2)_2]$ (**5**, Figure 9, red trace). To obtain further spectroscopic characterization, a sample containing ^{57}Fe-enriched **6**/**7** and 15 equiv of H_2O in tetrahydrofuran was studied by Mössbauer spectroscopy at 80 K (Figure S12C). The spectrum was fit to a single quadrupole doublet, with $\delta = 0.49(2)$ mm/s and $\Delta E_Q = 0.97(2)$ mm/s. These parameters are nearly identical to those obtained for **5** (Table 1). Although we are unable to crystallize this material, the spectroscopic data suggest that the compound has the molecular formula $[Fe_4(\mu\text{-OH})_6(PIM)_2(Ar^{Tol}CO_2)_2]$ (**8**).

The tendency for iron complexes to aggregate into clusters is well documented in the porphryin as well as the synthetic diiron literature.[79,81] Unlike the BMMs, which encapsulate their diiron cofactors within a protein matrix to avoid unwanted side reactions, small-molecule mimics do not have such exquisite steric protection. By installing bulkier groups around the PIM^{2-} ligand periphery, it should be possible to prevent formation of polynuclear species that lead to a dead-end in modeling studies. Having a "protected" ligand platform may also allow assembly of diiron(II) models using less sterically demanding carboxylates; this modification will reduce the steric congestion at the diiron core and may facilitate more facile reaction with external guests, such as O_2 and other substrates.

SUMMARY AND CONCLUSIONS

We designed a new macrocycle, H_2PIM, that can be prepared by a convenient multistep procedure in gram quantities. Reactions of H_2PIM with $[Fe_2(Mes)_4]$ in the presence of external carboxylates afford diiron(II) complexes that are excellent models for the reduced forms of the BMM active sites. These diiron(II) compounds react rapidly with dioxygen to give a variety of iron(III)-containing products, including (μ-hydroxo)diiron(III), (μ-oxo)diiron(III), and di(μ-hydroxo)diiron(III) complexes of direct relevance to the oxidized forms of the BMM diiron centers. Hexa(μ-hydroxo)tetrairon(III) complexes were also obtained. The composition of the oxygenation products is controlled in part by the nature of the external carboxylate ligand and the presence of water. These results demonstrate that the PIM^{2-} ligand is sufficiently preorganized to support a diiron core but, at the same time, sufficiently flexible to allow structural rearrangements at the metal center; this delicate balance has been difficult to achieve in prior diiron modeling chemistry.

The importance of this work is the demonstration that a macrocyclic framework can support carboxylate-bridged diiron cores in multiple oxidation states, enforce syn *N*-donor stereochemistry of two nitrogen ligands, supply two anionic oxygen atom donors, allow binding of two external carboxylates to the iron centers, have an internal cavity to form a quadrilateral $Fe_2(\mu\text{-}O)_2$ core, and be readily synthesized in gram quantities. To the best of our knowledge, no other ligand platform satisfies all of these design elements. As such, this study represents a significant step toward the ultimate goal of devising functional mimics of carboxylate-bridged diiron centers that occur at the active sites of many biologically essential metalloenzymes.

ASSOCIATED CONTENT

Supporting Information. Additional spectroscopic and electrochemical data, X-ray data collection and refinement details, a bond valence sum table, and partially labeled thermal ellipsoid diagrams of **1**−**7**, as well as the corresponding CIF files. This material is available free of charge via the Internet at http://pubs.acs.org.

AUTHOR INFORMATION

Corresponding Author
lippard@mit.edu

ACKNOWLEDGMENT

The work was supported by a grant GM032134 from the National Institute of General Medical Sciences. The authors thank Dr. Daniela Buccella for X-ray crystallographic assistance.

REFERENCES

(1) Feig, A. L.; Lippard, S. J. *Chem. Rev.* **1994**, *94*, 759–805.
(2) Wallar, B. J.; Lipscomb, J. D. *Chem. Rev.* **1996**, *96*, 2625–2658.
(3) Merkx, M.; Kopp, D. A.; Sazinsky, M. H.; Blazyk, J. L.; Müller, J.; Lippard, S. J. *Angew. Chem., Int. Ed.* **2001**, *40*, 2782–2807.
(4) Arenghi, F. L. G.; Berlanda, D.; Galli, E.; Sello, G.; Barbieri, P. *Appl. Environ. Microbiol.* **2001**, *67*, 3304–3308.
(5) Cafaro, V.; Izzo, V.; Scognamiglio, R.; Notomista, E.; Capasso, P.; Casbarra, A.; Pucci, P.; Di Donato, A. *Appl. Environ. Microbiol.* **2004**, *70*, 2211–2219.
(6) Cafaro, V.; Scognamiglio, R.; Viggiani, A.; Izzo, V.; Passaro, I.; Notomista, E.; Dal Piaz, F.; Amoresano, A.; Casbarra, A.; Pucci, P.; Di Donato, A. *Eur. J. Biochem.* **2002**, *269*, 5689–5699.
(7) Cadieux, E.; Vrajmasu, V.; Achim, C.; Powlowski, J.; Münck, E. *Biochemistry* **2002**, *41*, 10680–10691.
(8) Gallagher, S. C.; Cammack, R.; Dalton, H. *Eur. J. Biochem.* **1997**, *247*, 635–641.
(9) Hamamura, N.; Storfa, R. T.; Semprini, L.; Arp, D. J. *Appl. Environ. Microbiol.* **1999**, *65*, 4586–4593.
(10) Kotani, T.; Yamamoto, T.; Yurimoto, H.; Sakai, Y.; Kato, N. *J. Bacteriol.* **2003**, *185*, 7120–7128.
(11) Rosenzweig, A. C.; Nordlund, P.; Takahara, P. M.; Frederick, C. A.; Lippard, S. J. *Chem. Biol.* **1995**, *2*, 409–418.
(12) Rosenzweig, A. C.; Frederick, C. A.; Lippard, S. J.; Nordlund, P. *Nature* **1993**, *366*, 537–543.
(13) Rosenzweig, A. C.; Lippard, S. J. *Acc. Chem. Res.* **1994**, *27*, 229–236.
(14) Nordlund, P.; Reichard, P. *Annu. Rev. Biochem.* **2006**, *75*, 681–706.
(15) Vu, V. V.; Emerson, J. P.; Martinho, M.; Kim, Y. S.; Münck, E.; Park, M. H.; Que, L., Jr. *Proc. Natl. Acad. Sci. U.S.A.* **2009**, *106*, 14814–14819.
(16) Behan, R. K.; Lippard, S. J. *Biochemistry* **2010**, *49*, 9679–9681.
(17) Oldenhuis, R.; Vink, R. L. J.; Janssen, D. B.; Witholt, B. *Appl. Environ. Microbiol.* **1989**, *55*, 2819–2826.
(18) Fox, B. G.; Borneman, J. G.; Wackett, L. P.; Lipscomb, J. D. *Biochemistry* **1990**, *29*, 6419–6427.
(19) Canada, K. A.; Iwashita, S.; Shim, H.; Wood, T. K. *J. Bacteriol.* **2002**, *184*, 344–349.
(20) Tao, Y.; Fishman, A.; Bentley, W. E.; Wood, T. K. *J. Bacteriol.* **2004**, *186*, 4705–4713.
(21) Fishman, A.; Tao, Y.; Rui, L.; Wood, T. K. *J. Biol. Chem.* **2005**, *280*, 506–514.
(22) Cafaro, V.; Notomista, E.; Capasso, P.; Di Donato, A. *Appl. Environ. Microbiol.* **2005**, *71*, 4736–4743.
(23) Cafaro, V.; Notomista, E.; Capasso, P.; Di Donato, A. *Appl. Environ. Microbiol.* **2005**, *71*, 4744–4750.
(24) Du Bois, J.; Mizoguchi, T. J.; Lippard, S. J. *Coord. Chem. Rev.* **2000**, *200*−*202*, 443–485.
(25) Fontecave, M.; Ménage, S.; Duboc-Toia, C. *Coord. Chem. Rev.* **1998**, *178*−*180*, 1555–1572.
(26) Que, L., Jr.; Tolman, W. B. *Nature* **2008**, *455*, 333–340.
(27) Friedle, S.; Reisner, E.; Lippard, S. J. *Chem. Soc. Rev.* **2010**, *39*, 2768–2779.
(28) Siewert, I.; Limberg, C. *Chem.—Eur. J.* **2009**, *15*, 10316–10328.
(29) Rardin, R. L.; Tolman, W. B.; Lippard, S. J. *New J. Chem.* **1991**, *15*, 417–430.
(30) Tshuva, E. Y.; Lippard, S. J. *Chem. Rev.* **2004**, *104*, 987–1012.
(31) Armstrong, W. H.; Spool, A.; Papaefthymiou, G. C.; Frankel, R. B.; Lippard, S. J. *J. Am. Chem. Soc.* **1984**, *106*, 3653–3667.

(32) Dong, Y.; Yan, S.; Young, V. G., Jr.; Que, L., Jr. *Angew. Chem., Int. Ed.* **1996**, *35*, 618–620.
(33) Kim, K.; Lippard, S. J. *J. Am. Chem. Soc.* **1996**, *118*, 4914–4915.
(34) Ookubo, T.; Sugimoto, H.; Nagayama, T.; Masuda, H.; Sato, T.; Tanaka, K.; Maeda, Y.; Ōkawa, H.; Hayashi, Y.; Uehara, A.; Suzuki, M. *J. Am. Chem. Soc.* **1996**, *118*, 701–702.
(35) LeCloux, D. D.; Barrios, A. M.; Lippard, S. J. *Bioorg. Med. Chem.* **1999**, *7*, 763–772.
(36) Dong, Y.; Ménage, S.; Brennan, B. A.; Elgren, T. E.; Jang, H. G.; Pearce, L. L.; Que, L., Jr. *J. Am. Chem. Soc.* **1993**, *115*, 1851–1859.
(37) Kuzelka, J.; Farrell, J. R.; Lippard, S. J. *Inorg. Chem.* **2003**, *42*, 8652–8662.
(38) Kodanko, J. J.; Morys, A. J.; Lippard, S. J. *Org. Lett.* **2005**, *7*, 4585–4588.
(39) Kodanko, J. J.; Lippard, S. J. *Inorg. Chim. Acta* **2008**, *361*, 894–900.
(40) Do, L. H.; Lippard, S. J. *Inorg. Chem.* **2009**, *48*, 10708–10719.
(41) Chen, C.-T.; Siegel, J. S. *J. Am. Chem. Soc.* **1994**, *116*, 5959–5960.
(42) Klose, A.; Solari, E.; Floriani, C.; Chiesi-Villa, A.; Rizzoli, C.; Re, N. *J. Am. Chem. Soc.* **1994**, *116*, 9123–9135.
(43) Sheldrick, G. M. *SADABS*, Area-Detector Absorption Corrrection; University of Göttingen: Göttingen, Germany, 2001.
(44) Sheldrick, G. M. *Acta Crystallogr., Sect. A* **2008**, *A64*, 112–122.
(45) Spek, A. L. *PLATON*, A Multipurpose Crystallographic Tool; Utrecht University: Utrecht, The Netherlands, 2000.
(46) Ambrosi, G.; Formica, M.; Fusi, V.; Giorgi, L.; Micheloni, M. *Coord. Chem. Rev.* **2008**, *252*, 1121–1152.
(47) Bordwell, F. G.; Algrim, D. *J. Org. Chem.* **1976**, *41*, 2507–2508.
(48) Bordwell, F. G.; McCallum, R. J.; Olmstead, W. N. *J. Org. Chem.* **1984**, *49*, 1424–1427.
(49) Shu, L.; Nesheim, J. C.; Kauffmann, K.; Münck, E.; Lipscomb, J. D.; Que, L., Jr. *Science* **1997**, *275*, 515–518.
(50) Kimura, S.; Bill, E.; Bothe, E.; Weyhermüller, T.; Weighardt, K. *J. Am. Chem. Soc.* **2001**, *123*, 6025–6039.
(51) Sessler, J. L.; Tomat, E.; Mody, T. D.; Lynch, V. M.; Veauthier, J. M.; Mirsaidov, U.; Markert, J. T. *Inorg. Chem.* **2005**, *44*, 2125–2127.
(52) Tomat, E.; Cuesta, L.; Lynch, V. M.; Sessler, J. L. *Inorg. Chem.* **2007**, *46*, 6224–6226.
(53) Borovik, A. S.; Papaefthymiou, V.; Taylor, L. F.; Anderson, O. P.; Que, L., Jr. *J. Am. Chem. Soc.* **1989**, *111*, 6183–6195.
(54) Cox, D. D.; Benkovic, S. J.; Bloom, L. M.; Bradley, F. C.; Nelson, M. J.; Que, L. Jr.; Wallick, D. E. *J. Am. Chem. Soc.* **1988**, *110*, 2026–2032.
(55) Koch, S. A.; Millar, M. *J. Am. Chem. Soc.* **1982**, *104*, 5255–5257.
(56) Pyrz, J. W.; Roe, A. L.; Stern, L. J.; Que, L., Jr. *J. Am. Chem. Soc.* **1985**, *107*, 614–620.
(57) Although there is an ambiguity in fitting Mössbauer data containing overlapping quadrupole doublets with equal intensities, we favor the current model because the chemically distinct four- and five-coordinate iron atoms in **1** should give rise to different δ values. We have not excluded the alternate model, however, which would afford similar δ but different ΔE_Q parameters.
(58) Yoon, S.; Lippard, S. J. *J. Am. Chem. Soc.* **2005**, *127*, 8386–8397.
(59) Liu, K. E.; Valentine, A. M.; Wang, D.; Huynh, B. H.; Edmondson, D. E.; Salifoglou, A.; Lippard, S. J. *J. Am. Chem. Soc.* **1995**, *117*, 10174–10185.
(60) DeWitt, J. G.; Bentsen, J. G.; Rosenzweig, A. C.; Hedman, B.; Green, J.; Pilkington, S.; Papaefthymiou, G. C.; Dalton, H.; Hodgson, K. O.; Lippard, S. J. *J. Am. Chem. Soc.* **1991**, *113*, 9219–9235.
(61) Stoian, S. A.; Smith, J. M.; Holland, P. L.; Münck, E.; Bominaar, E. L. *Inorg. Chem.* **2008**, *47*, 8687–8695.
(62) Hu, C.; Sulok, C. D.; Paulat, F.; Lehnert, N.; Twigg, A. I.; Hendrich, M. P.; Schulz, C. E.; Scheidt, W. R. *J. Am. Chem. Soc.* **2010**, *132*, 3737–3750.
(63) Bertini, I.; Luchinat, C. In *Physical Methods For Chemists*; Drago, R. S., Ed.; Surfside Scientific Publishers: Gainsville, FL, 1992; pp 500−558.
(64) Iggo, J. A. *NMR Spectroscopy in Inorganic Chemistry*; Oxford University Press, Inc.: New York, 1999.
(65) Adam, B.; Bill, E.; Bothe, E.; Goerdt, B.; Haselhorst, G.; Hildenbrand, K.; Sokolowski, A.; Steenken, S.; Weyhermüller, T.; Wieghardt, K. *Chem.—Eur. J.* **1997**, *3*, 308–319.
(66) Roy, N.; Sproules, S.; Weyhermüller, T.; Wieghardt, K. *Inorg. Chem.* **2009**, *48*, 3783–3791.
(67) Strautmann, J. B. H.; Freiherr von Richthofen, C.-G.; George, S. D.; Bothe, E.; Bill, E.; Glaser, T. *Chem Commun.* **2009**, 2637–2639.
(68) Connelly, N. G.; Geiger, W. E. *Chem. Rev.* **1996**, *96*, 877–910.
(69) Sanders-Loehr, J.; Wheeler, W. D.; Shiemke, A. K.; Averill, B. A.; Loehr, T. M. *J. Am. Chem. Soc.* **1989**, *111*, 8084–8093.
(70) Kurtz, D. M., Jr. *Chem. Rev.* **1990**, *90*, 585–606.
(71) Kang, H. C.; Hanson, A. W.; Eaton, B.; Boekelheide, V. *J. Am. Chem. Soc.* **1985**, *107*, 1979–1985.
(72) Xu, W.; Puddephatt, R. J.; Muir, K. W.; Torabi, A. A. *Organometallics* **1994**, *13*, 3054–3062.
(73) Ning, G. L.; Wu, L. P.; Sugimoto, K.; Munakata, M.; Kuroda-Sowa, T.; Maekawa, M. *J. Chem. Soc., Dalton Trans.* **1999**, 2529–2536.
(74) Altermatt, D.; Brown, I. D. *Acta Crystallogr.* **1985**, *B41*, 240–244.
(75) Thorp, H. H. *Inorg. Chem.* **1992**, *31*, 1585–1588.
(76) Drago, R. S. In *Physical Methods For Chemists*; Surfside Scientific Publishers: Gainsville, FL, 1992; pp 626−649.
(77) Boudalis, A. K.; Clemente-Juan, J. M.; Dahan, F.; Psycharis, V.; Raptopoulou, C. P.; Donnadieu, B.; Sanakis, Y.; Tuchagues, J.-P. *Inorg. Chem.* **2008**, *47*, 11314–11323.
(78) Uehara, K.; Mizuno, N. *J. Am. Chem. Soc.* **2011**, *133*, 1622–1625.
(79) Collman, J. P.; Gagne, R. R.; Reed, C. A.; Halbert, T. R.; Lang, G.; Robinson, W. T. *J. Am. Chem. Soc.* **1975**, *97*, 1427–1439.
(80) Lippard, S. J. *Angew. Chem., Int. Ed.* **1988**, *27*, 344–361.
(81) Chen, Q.; Lynch, J. B.; Gomez-Romero, P.; Ben-Hussein, A.; Jameson, G. B.; O'Connor, C. J.; Que, L., Jr. *Inorg. Chem.* **1988**, *27*, 2673–2681.